National Research Council Canada
Conseil national de recherches Canada

AEROELASTIC RESPONSE OF AN AIRCRAFT WING TO RANDOM LOADS

by
B.H.K. Lee
National Aeronautical Establishment

OTTAWA
APRIL 1983

Canada

AERONAUTICAL REPORT
LR-613
NRC NO. 21230

86-02699/

NATIONAL AERONAUTICAL ESTABLISHMENT

SCIENTIFIC AND TECHNICAL PUBLICATIONS

AERONAUTICAL REPORTS:

Aeronautical Reports (LR): Scientific and technical information pertaining to aeronautics considered important, complete, and a lasting contribution to existing knowledge.

Mechanical Engineering Reports (MS): Scientific and technical information pertaining to investigations outside aeronautics considered important, complete, and a lasting contribution to existing knowledge.

AERONAUTICAL NOTES (AN): Information less broad in scope but nevertheless of importance as a contribution to existing knowledge.

LABORATORY TECHNICAL REPORTS (LTR): Information receiving limited distribution because of preliminary data, security classification, proprietary, or other reasons.

Details on the availability of these publications may be obtained from:

Publications Section,
National Research Council Canada,
National Aeronautical Establishment,
Bldg. M-16, Room 204,
Montreal Road,
Ottawa, Ontario
K1A 0R6

ÉTABLISSEMENT AÉRONAUTIQUE NATIONAL

PUBLICATIONS SCIENTIFIQUES ET TECHNIQUES

RAPPORTS D'AÉRONAUTIQUE

Rapports d'néronautique (LR): Informations scientifiques et techniques touchant l'aéronautique jugées importantes, complètes et durables en termes de contribution aux connaissances actuelles.

Rapports de génie mécanique (MS). Informations scientifiques et techniques sur la recherche externe à l'aéronautique jugées importantes, complètes et durables en termes de contribution aux connaissances actuelles.

CAHIERS D'AÉRONAUTIQUE (AN): Informations de moindre portée mais importantes en termes d'accroissement des connaissances.

RAPPORTS TECHNIQUES DE LABORATOIRE (LTR): Informations peu disséminées pour des raisons d'usage secret, de droit de propriété ou autres ou parce qu'elles constituent des données préliminaires.

Les publications ci-dessus peuvent être obtenues à l'adresse suivante:

Section des publications
Conseil national de recherches Canada
Établissement aéronautique national
Im. M-16, pièce 204
Chemin de Montréal
Ottawa (Ontario)
K1A 0R6

AEROELASTIC RESPONSE OF AN AIRCRAFT WING TO RANDOM LOADS

RÉPONSE AÉROÉLASTIQUE D'UNE AILE D'AÉRONEF À DES CHARGES ALÉATOIRES

by/par

B.H.K. Lee

L.H. Ohman, Head/Chef
High Speed Aerodynamics Laboratory/
Laboratoire d'aérodynamique à hautes vitesses

G.M. Lindberg
Director/Directeur

SUMMARY

A method for the prediction of the response of an elastic wing to random loads at flight conditions using rigid model wind tunnel pressure fluctuation measurements is presented. The wing is divided into panels or elements, and the load is computed from measured pressure fluctuations at the centre of each panel. A series representation with terms of the correlated noise type is used to curve fit the experimentally determined pressure power spectra. Two methods are used to calculate the random load spectrum: a constant correlation approximation, and an exponential spatially decaying cross-power spectrum model for the pressure. The coupling between the structural dynamics and aerodynamics of a vibrating wing is taken into consideration using the doublet-lattice method for computing the unsteady aerodynamic forces. The acceleration and displacement response spectra have been computed for the F-4E aircraft for various Mach numbers, dynamic pressures and flight altitudes. The importance of the unsteady aerodynamic loads induced by the vibration of the wing and input load representation is illustrated by comparing the theoretical predictions with results from flight tests.

RÉSUMÉ

Il s'agit d'une méthode pour prédire la réponse d'une aile élastique à des charges aléatoires en vol à partir des mesures de fluctuations de pression sur une maquette rigide en soufflerie. L'aile est divisée en panneaux ou éléments, et la charge est calculée à partir des mesures de fluctuations de pression prises au centre de chaque panneau. Une représentation série des termes du type de bruit en corrélation sert à tracer la courbe des spectres de puissance pression déterminés expérimentalement. Deux méthodes sont employées pour calculer le spectre des charges aléatoires: l'approximation par corrélation des constantes et un modèle exponentiel du spectre de la puissance décroissante dans l'espace pour la pression. La relation entre la dynamique structurale et l'aérodynamique d'une aile en vibration est prise en compte au moyen de la méthode de réseau des doublets pour calculer les forces aérodynamiques variables. Les spectres de réponse en accélération et en déplacement ont été calculés pour le chasseur F-4E à divers nombres de Mach, diverses pressions dynamiques et altitudes de vol. L'importance des charges aérodynamiques variables induites par la vibration de l'aile et la représentation des charges exercées est démontrée par la comparaison des prédictions théoriques avec les résultats des vols d'essai.

CONTENTS

		Page
SUMMARY		(iii)
SYMBOLS		(vi)
1.0 INTRODUCTION		1
2.0 ANALYSIS		1
2.1 Dynamic Aeroelastic Equations		1
2.2 Representation of External Load on Wing		3
2.3 The Doublet-Lattice Method		4
2.4 Coupling between Structural Dynamics and Unsteady Aerodynamics for a Vibrating Wing		5
3.0 RESULTS AND DISCUSSIONS		6
4.0 CONCLUSIONS		9
5.0 REFERENCES		9
APPENDIX A	Expressions for K_1 and K_2 in the Equation for Normalwash	47
APPENDIX B	Expressions for Normalwash Factor	49

ILLUSTRATIONS

Figure		Page
1	Schematic of Wing	13
2	Panel Representation of Wing	14
3	Representation of Wing by Panels and Location of Vortices, Doublets and Collocation Points	15
4	Wing and Element Co-Ordinates	16
5	Block Diagram for Wing Response to Random Loading	17
6	Panel Representation of F-4E Wing Planform	18
7	Approximate Modelling of RMS Pressure Coefficient on Wing	19
8	Pressure Transducer Locations	20

ILLUSTRATIONS (Cont'd)

Figure		Page
9	Comparison of Response Acceleration Power Spectral Density from Flight Tests with Theoretical Predictions Using Constant Correlation Assumption at M = 0.78 and Q = 220 psf	21
10	Comparison of Response Acceleration Power Spectral Density from Flight Tests with Theoretical Predictions Using Constant Correlation Assumption at M = 0.82 and Q = 350 psf	22
11	Variation of Acceleration Power Spectral Density with Mach Number and Flight Altitude for Q = 220 psf	23
12	Variation of Displacement Power Spectral Density with Mach Number and Flight Altitude for Q = 220 psf	24
13	Variation of Acceleration Power Spectral Density with Mach Number and Flight Altitude for Q = 350 psf	25
14	Variation of Displacement Power Spectral Density with Mach Number and Flight Altitude for Q = 350 psf	26
15	Variation of Acceleration Power Spectral Density with Dynamic Pressure and Flight Altitude for M = 0.51	27
16	Variation of Displacement Power Spectral Density with Dynamic Pressure and Flight Altitude for M = 0.51	28
17	Variation of Acceleration Power Spectral Density with Dynamic Pressure and Flight Altitude for M = 0.78	29
18	Variation of Displacement Power Spectral Density with Dynamic Pressure and Flight Altitude for M = 0.78	30
19	Variation of Acceleration Power Spectral Density Normalized with Respect to Q^2 with Dynamic Pressure and Flight Altitude for M = 0.51	31
20	Variation of Displacement Power Spectral Density Normalized with Respect to Q^2 with Dynamic Pressure and Flight Altitude for M = 0.51	32
21	Variation of Acceleration Power Spectral Density Normalized with Respect to Q^2 with Dynamic Pressure and Flight Altitude for M = 0.78	33
22	Variation of Displacement Power Spectral Density Normalized with Respect to Q^2 with Dynamic Pressure and Flight Altitude for M = 0.78	34
23	Variation of Acceleration Power Spectral Density with Mach Number and Dynamic Pressure at 15,000 ft. Altitude	35
24	Variation of Displacement Power Spectral Density with Mach Number and Dynamic Pressure at 15,000 ft. Altitude	36

ILLUSTRATIONS (Cont'd)

Figure		Page
25	Variation of Acceleration Power Spectral Density with Structural Damping for M = 0.78, Q = 220 psf	37
26	Variation of Displacement Power Spectral Density with Structural Damping for M = 0.78, Q = 220 psf	38
27	Variation of Acceleration Power Spectral Density with Structural Damping for M = 0.82, Q = 350 psf	39
28	Variation of Displacement Power Spectral Density with Structural Damping for M = 0.82, Q = 350 psf	40
29	Comparison of Response Acceleration Power Spectral Density from Flight Tests with Theoretical Predictions Using Exponential Spatially Decaying Pressure Cross-Spectrum Assumption for M = 0.78, Q = 220 pf	41
30	Displacement Power Spectral Density Using Exponential Spatially Decaying Pressure Cross-Spectrum Assumption for M = 0.78, Q = 220 pf	42
31	Comparison of Response Acceleration Power Spectral Density from Flight Tests with Theoretical Predictions Using Exponential Spatially Decaying Pressure Cross-Spectrum Assumption for M = 0.82, Q = 350 psf	43
32	Displacement Power Spectral Density Using Exponential Spatially Decaying Pressure Cross-Spectrum Assumption for M = 0.82, Q = 350 psf	44
33	Comparison of Response Acceleration Power Spectral Density from Flight Tests with Theretical Predictions for M = 0.78, Q = 220 psf	45
34	Comparison of Response Acceleration Power Spectral Density from Flight Tests with Theoretical Predictions for M = 0.82, Q = 350 psf	46
B1	Horseshoe Vortex System	52

SYMBOLS

Symbol	Definition
A	area of a panel
b	wing semi-span
C	generalized damping coefficient
$\bar{c}$	average chord
D	normalwash factor

SYMBOLS (Cont'd)

Symbol	Definition
D_0	steady normalwash factor
D_1	planar normalwash factor
D_2	non-planar normalwash factor
E	defined in Equation (38)
e	semiwidth of panel
f	frequency
H	frequency response function
I	defined in Equation (19)
K	defined in Equation (35), also generalized stiffness
K_1,K_2	defined in Equations (A1) and (A2) respectively
k	reduced frequency
L	Fourier transform of generalized load
ℓ	generalized load
M	Mach number
P	Fourier transform of pressure
p	pressure
Q	Fourier transform of displacement in generalized co-ordinates, also dynamic pressure
q	generalized co-ordinate
r	distance between centres of two panels
S_L	load spectrum
S_p	pressure spectrum
S_Q	spectrum of displacement in generalized co-ordinates
T_1, T_2	defined in Equations (23) and (24) respectively
t	time
U	free stream velocity

SYMBOLS (Cont'd)

Symbol	Definition
U_c	convection velocity
w	normalwash
W	Fourier transform of normalwash
x,y,z	Cartesian co-ordinate system
X	panel dimension in x-direction, also frequency parameter defined in Equation (41)
Δx_s	chord of sending panel
Y	dimension of panel in y-direction
z	displacement in z-direction
α	decay coefficient in x-direction
β	decay coefficient in y-direction
γ	dihedral angle of sending and receiving point
δ	boundary layer thickness
ζ	damping ratio
η	co-ordinate (in y-direction)
λ	sweep angle of panel quarter-chord
ξ	co-ordinate (in x-direction)
ρ	density
ϕ	mode shape function
ω	frequency
ω_n	natural frequency

Subscripts

L	denotes applied load
'r','s'	denotes receiving and sending point
'k'	denotes the k-th panel
'α','β'	denotes the α and β mode of vibration

SYMBOLS (Cont'd)

Symbol	Definition
Superscripts	
'k'	denotes the k-th panel
'r'	denotes the r-th panel
'D'	denotes random component of load due to wing buffeting or turbulence
'A'	denotes unsteady aerodynamic component of load due to vibration of wing
'′'	denotes non-dimensional quantities

AEROELASTIC RESPONSE OF AN AIRCRAFT WING TO RANDOM LOADS

1.0 INTRODUCTION

In References 1 and 2 the dynamic response of a wing to statistical non-stationary random loads is investigated using a time-segmentation technique. The time history of the applied load is segmented into a number of time intervals. In each time segment the non-stationary load is represented by the product of a deterministic shaping function and a statistically stationary random function. The total response is obtained by summation of the responses of the wing from each time segment. This approach is useful when the aircraft engages in rapid manoeuvres. Because of the complexities of the analysis only the structural response, without consideration of the unsteady aerodynamics around the vibrating wing, is analyzed. It is assumed that aerodynamic effects can be approximately accounted for by using a damping value in the dynamic aerolastic equations that is determined either experimentally or from estimation.

In order to make the problem of the coupling between structural dynamics and aerodynamics of a vibrating wing more amenable to theoretical analysis, the random loading on the wing is assumed to be statistically stationary. This assumption can be justified as long as the flight conditions are unchanged within a reasonably long analysis time, when measurements are made of either the load or the wing response. In wind tunnel testing statistical stationarity requires long running time compared to the natural period of the mode of vibration under investigation. The random loads experienced by a wing of an aircraft arise from turbulence or flow separation at buffet conditions. The use of statistical theory in the investigation of buffeting was pioneered by Liepman (Ref. 3) who examined the problem of the lift force exerted on a two-dimensional thin airfoil moving in turbulent air. Later, he extended the method to wings of finite span (Ref. 4). The analysis was generalized by Ribner (Ref. 5) using a model of turbulence represented by the superposition of plane sinusoidal shear waves of all arientations and wavelengths. The correlations between flight and wind tunnel tests with predictions based on statistical approach had been reported by various investigators (Refs. 6-10). Amongst the more recent studies in this subject are those of Mullan and Lemley (Ref. 11), Hwang and Pi (Refs. 12, 13), Jones (Ref. 14) and Butler and Spavins (Ref. 15). All the above studies consider only the structural response without including the effects of the unsteady aerodynamics around the vibrating wing. In this report, the method of Reference 2 is extended to include the coupling between the structural vibration and aerodynamics of a wing under random loading. The panel method described in Reference 2, which is a modification of a method proposed by Schweiker and Davis (Ref. 16) for the study of the response of shells to aerodynamic noise, is most suitable for adapting the doublet-lattice technique (Refs. 17-19) in computing the unsteady aerodynamics.

2.0 ANALYSIS

2.1 Dynamic Aeroelastic Equations

Consider a Cartesian co-ordinate system x, y and z fixed on the wing as illustrated in Figure 1. The displacement of the wing can be expressed in terms of a set of normal co-ordinates $q_\alpha(t)$ as:

$$z(x,y,t) = \sum_{\alpha=1}^{I} \phi_\alpha(x,y) q_\alpha(t) \qquad (1)$$

where $\phi_\alpha(x,y)$ is the mode shape function of the αth mode, and I is the number of modes required to adequately represent z(x,y,t) in the form of a series. The dynamic aeroelastic equations governing the response of $q_\alpha(t)$ to a load $\ell_\alpha(t)$ is given in generalized co-ordinate as:

$$M_\alpha \ddot{q}_\alpha + C_\alpha \dot{q}_\alpha + K_\alpha q_\alpha = \ell_\alpha(t) \qquad (2)$$

for the αth mode. The dots denotes differentiation with respect to time, M_α, C_α and K_α are the generalized mass, damping coefficient and stiffness of the αth mode respectively. In the above equation the assumption of light damping is made, thus cross damping terms do not appear.

Define the undamped natural frequency ω_{n_α} as:

$$\omega_{n_\alpha}^2 = \frac{K_\alpha}{M_\alpha} \tag{3}$$

and the damping ratio ζ_α as:

$$\zeta_\alpha = \frac{C_\alpha}{2\sqrt{M_\alpha K_\alpha}} \tag{4}$$

Using the above two expressions Equation (2) can be rewritten as follows:

$$\ddot{q}_\alpha + 2\zeta_\alpha \omega_{n_\alpha} \dot{q}_\alpha + \omega_{n_\alpha}^2 q_\alpha = \frac{1}{M_\alpha} \ell_\alpha(t) \tag{5}$$

The generalized force can be expressed in terms of the fluctuating pressure p(x,y,t) as:

$$\ell_\alpha(t) = \iint_{\substack{\text{wing} \\ \text{planform}}} \phi_\alpha(x,y) p(x,y,t) dxdy \tag{6}$$

where the integration is taken over the wing surface. Let $L_\alpha(\omega)$, $Q_\alpha(\omega)$ and $P(x,y,\omega)$ be the Fourier transform of $\ell_\alpha(t)$, $q_\alpha(t)$ and $p(x,y,t)$ respectively, and introduce a frequency response function $H_\alpha(\omega)$ defined by:

$$H_\alpha(\omega) = \frac{1}{M_\alpha \left[\omega_{n_\alpha}^2 - \omega^2 + i2\zeta_\alpha \omega \omega_{n_\alpha}\right]} \tag{7}$$

Equation (5) can be written as follows:

$$Q_\alpha(\omega) = H_\alpha(\omega) L_\alpha(\omega) \tag{8}$$

In the term $\ell_\alpha(t)$ there are two types of forces acting on the surface of the wing. Let the component of the load due to buffeting or turbulence be represented by $\ell_\alpha^D(t)$ and that from the unsteady aerodynamic forces due to vibration of the wing be $\ell_\alpha^A(t)$, then

$$\ell_\alpha(t) = \ell_\alpha^D(t) + \ell_\alpha^A(t) \tag{9}$$

Similarly, the pressure can be expressed as

$$p(x,y,t) = p^D(x,y,t) + p^A(x,y,t) \tag{10}$$

and Equation (10) becomes

$$Q_\alpha(\omega) = H_\alpha(\omega) \left(L_\alpha^D(\omega) + L_\alpha^A(\omega)\right) \tag{11}$$

where $L_\alpha^D(\omega)$ and $L_\alpha^A(\omega)$ are the Fourier transforms of $\ell_\alpha^D(t)$ and $\ell_\alpha^A(t)$ respectively.

2.2 Representation of External Load on Wing

From Equation (6), the generalized force due to the random loading can be expressed in terms of the pressure $p^D(x,y,t)$ as follows:

$$\ell_\alpha^D(t) = \iint_{\substack{\text{wing}\\ \text{planform}}} \phi_\alpha(x,y)p^D(x,y,t)dxdy \tag{12}$$

The power spectral density can be written as:

$$S_{L_\alpha^D}(\omega) = \iiiint \phi_\alpha(x_1,y_1)\,\phi_\alpha(x_2,y_2)\,S_{p^D}(x_1,y_1,x_2,y_2,\omega)\,dx_1,dy_1,dx_2,dy_2 \tag{13}$$

where $S_{p^D}(x_1,y_1,x_2,y_2,\omega)$ is the cross power spectral density of the pressure $p^D(x,y,t)$ between points (x_1,y_1) and (x_2,y_2) (Fig. 1).

In Figure 2 a panel representation of the wing is shown. From Reference 2, $S_{L_\alpha^D}(\omega)$ can be written as:

$$S_{L_\alpha^D}(\omega) = \sum_{k=1}^{K} \left(\bar{\phi}_\alpha^k\right)^2 \int_{A_K}\int S_{p^D}(x_1,y_1,x_2,y_2,\omega)dA_k\,dA_k \tag{14}$$

where A_k is the area of the k-th panel and $\bar{\phi}_\alpha^k$ is an average mode shape for the 'α' mode within the k-th panel defined by

$$\bar{\phi}_\alpha^k = \frac{1}{A_k}\int_{A_K} \phi_\alpha(x,y)dA_k \tag{15}$$

When the distance $r_{k\ell}$ (Fig. 2) between the centres of the k-th and ℓ-th panels is large (Ref. 2), an approximate form for $S_{L_\alpha^D}(\omega)$ at very low vibration frequencies can be obtained by assuming the pressure at the centre of a panel to be representative of the pressure field at all points within that panel. The pressure spectrum at any point is given by that at the centre of the panel and the pressure cross spectrum between two points in the same panel is taken to be equal to the pressure spectrum at the panel centre. Equation (14) can then be simplified to the following:

$$S_{L_\alpha^D}(\omega) = \sum_{k=1}^{K} S_{p^D}^k(\omega)\left(\bar{\phi}_\alpha^k\right)^2 A_k^2 \tag{16}$$

where $S_{p^D}^k(\omega)$ is the pressure spectrum at the centre of the k-th panel. A more accurate expression for $S_{L_\alpha^D}(\omega)$ can be obtained by writing $S_{p^D}(x_1,y_1,x_2,y_2,\omega)$ as follows:

$$S_{p^D}(x_1,y_1,x_2,y_2,\omega) = S_{p^D}^k(\omega)\, e^{-\alpha|x_1-x_2|}\, e^{-\beta|y_1-y_2|}\cos p(x_1 - x_2) \tag{17}$$

where α and β are spatial decay coefficients in the x and y directions respectively, $p = \frac{\omega}{U_c}$, and U_c is the convection velocity. Substituting Equation (17) into Equation (16) and carrying out the integration gives the following:

$$S_{L_\alpha^D}(\omega) = \sum_{k=1}^{K} S^k_{p^D}(\omega) \left(\bar{\phi}^k_\alpha\right)^2 I^k \tag{18}$$

where

$$I^k = \frac{4}{\beta^2} \frac{(e^{-\beta Y^k} + \beta Y^k - 1)}{(\alpha^2 + p^2)^2} \left\{ p^2 - \alpha^2 + \alpha X^k(\alpha^2 + p^2) + e^{-\alpha X^k} \left[(\alpha^2 - p^2)\cos pX^k - 2\alpha p \sin pX^k\right]\right\} \tag{19}$$

and X^k and Y^k are the dimensions of the k-th panel (Fig. 2).

2.3 The Doublet-Lattice Method

The doublet-lattice method is described in References 17-19, and in this report, only a brief outline of the method and the equations needed in the present analysis will be given.

The wing surface is divided into small elements or panels arranged in strips parallel to the free stream and all surface edges, fold lines and hinge lines lie on the panel boundaries (Fig. 3). In each panel the steady flow is represented by a horseshoe vortex having the bound vortex of the horseshoe system lying along the quarter-chord line. Superimposed on the bound vortex are acceleration potential doublets of uniform strength. The control point is located at the three-quarter chord point. The normalwash w_r' at panel 'r' non-dimensionalized with respect to the free stream velocity U is given by the following:

$$w_r' = \sum_s D_{rs} \Delta C_{ps} \tag{20}$$

where D_{rs} is the normalwash factor, and the summation is over all the panels. In a co-ordinate system having the midpoint of the sending element as origin and the axes aligned with the sending element (Fig. 4), the normalwash factor can be written as (Ref. 20):

$$D_{rs} = \frac{\Delta x_s}{8} \int_{-e}^{e} \left(\frac{K_1 T_1}{r_1^2} + \frac{K_2 T_2}{r_1^4}\right) \exp\left[-i\omega(\bar{x} - \bar{\eta}\tan\lambda_s)/U\right] d\bar{\eta} \tag{21}$$

where

$$r_1 = \left[(\bar{y} - \bar{\eta})^2 + \bar{z}^2\right]^{1/2} \tag{22}$$

Δx_s is the chord of the sending panel (Fig. 3), λ_s is the sweep angle of its quarter-chord, and e is its semi-width. T_1 and T_2 are the direction cosine functions given as:

$$T_1 = \cos(\gamma_s - \gamma_r) \tag{23}$$

$$T_2 = \bar{z}\left[\bar{z}\cos(\gamma_s - \gamma_r) + (\bar{y} - \bar{\eta})\sin(\gamma_s - \gamma_r)\right] \tag{24}$$

where γ_s and γ_r are the dihedral angles at the sending and receiving points on the respective panels. K_1 and K_2 are given in Appendix A. Equation (21) can be written in the following form:

$$D_{rs} = D_{0_{rs}} + D_{1_{rs}} + D_{2_{rs}} \tag{25}$$

where $D_{0_{rs}}$, $D_{1_{rs}}$ and $D_{2_{rs}}$ are the steady, planar and non-planar normalwash factors respectively, given in Appendix B.

The normalwash boundary conditions for the lifting surface elements are determined by assuming the surfaces to move normal to themselves. Taking the substantial derivative of Equation (1), the normalwash at panel 'r' is:

$$w_r'(t) = \sum_\alpha w_{r\alpha}'(t) \tag{26}$$

and

$$w_{r_\alpha}'(t) = \left(\frac{1}{U}\frac{\partial}{\partial t} + \frac{\partial}{\partial x}\right) z_\alpha'(x,y,t) \tag{27}$$

where

$$k = \frac{\omega \bar{c}}{U} \tag{28}$$

$\bar{c}$ is the average chord and the $'$ denotes non-dimensional quantities. The Fourier transform of Equation (27) gives:

$$W_{r_\alpha}'(\omega) = \left(\frac{\partial \phi_\alpha^r}{\partial x'} + ik\,\phi_\alpha^r\right) Q_\alpha'(\omega) \tag{29}$$

2.4 Coupling between Structural Dynamics and Unsteady Aerodynamics for a Vibrating Wing

The external loading on the wing due either to buffeting or turbulence causes vibration of the wing which in turn generates unsteady aerodynamic forces on the wing surface. Figure 5 shows a block diagram illustrating the procedure in calculating the response of a wing to random loading with the aerodynamics included in a feedback loop. The aerodynamic load $L_\alpha^A(\omega)$ can be written as:

$$L_\alpha^A(\omega) = \iint_{\substack{\text{wing}\\ \text{planform}}} \phi_\alpha(x,y) P(x,y,\omega)\,dx\,dy \tag{30}$$

where

$$P(x,y,\omega) = \sum_\beta P_\beta(x,y,\omega) Q_\beta(\omega) \tag{31}$$

$P(x,y,\omega)$ is the Fourier transform of $p^A(x,y,t)$ in Equation (10). Evaluating Equation (30) over each panel and summing over all panels, $L_\alpha^A(\omega)$ becomes:

$$L_\alpha^A(\omega) = \frac{1}{2}\rho U^2 \bar{c}^2 \sum_\beta \sum_k \bar{\phi}_\alpha^k \Delta C_{p_\beta}^k A_k' Q_\beta'(\omega) \tag{32}$$

where $'$ denotes non-dimensional quantities and ΔC_p is the pressure coefficient.

The power spectrum $S_{L_\alpha^A}(\omega)$ of the aerodynamic load can be written as:

$$S_{L_\alpha^A}(\omega) = \left(\frac{1}{2}\rho U^2 \bar{c}^2\right)^2 \sum_k \sum_\beta \left(\bar{\phi}_\alpha^k\right)^2 \Delta C_{p_\beta}^k(\omega)\, \Delta C_{p_\beta}^{*k}(\omega)\, S_{Q_\beta'}(\omega)\, A_k'^2 \tag{33}$$

where $S_{Q'_\beta}(\omega)$ is the power spectral density of $Q'_\beta(\omega)$ and * denotes the complex conjugate.

In non-dimensional form, Equation (8) can be re-written as:

$$Q'_\alpha(\omega) = K_\alpha H'_\alpha(\omega) \left\{ L'^{A}_\alpha(\omega) + L'^{D}_\alpha(\omega) \right\} \tag{34}$$

where

$$K_\alpha = \frac{1}{2} \frac{\rho U^2 \bar{c}}{M_\alpha \omega_{n_\alpha}^2} \tag{35}$$

and

$$H'_\alpha(\omega) = \left\{ 1 - \left(\frac{\omega}{\omega_{n_\alpha}} \right)^2 + i2\zeta_\alpha \frac{\omega}{\omega_{n_\alpha}} \right\}^{-1} \tag{36}$$

The primed quantities for the loads are non-dimensional with respect to $\frac{1}{2}\rho U^2 \bar{c}^2$. Using Equation (32) an expression for $S_{Q'_\alpha}(\omega)$ can be obtained from the following:

$$S_{Q'_\alpha}(\omega) \left\{ 1 - H'_\alpha(\omega) E_{\alpha\alpha}(\omega) - H'^{*}_\alpha(\omega) E^{*}_{\alpha\alpha}(\omega) + \left| H'_\alpha(\omega) \right|^2 \left| E_{\alpha\alpha}(\omega) \right|^2 \right\}$$

$$+ \left| H'_\alpha(\omega) \right|^2 \sum_{\substack{\beta \\ \beta \neq \alpha}} \left| E_{\beta\alpha}(\omega) \right|^2 S_{Q'_\beta}(\omega) = \left| H'_\alpha(\omega) \right|^2 K_\alpha^2 S_{L'_\alpha{}^{D}}(\omega) \tag{37}$$

where

$$E_{\alpha\beta}(\omega) = K_\alpha \sum_k \bar{\phi}^k_\alpha \Delta C^k_{p_\beta}(\omega) A'_k \tag{38}$$

To determine $\Delta C^k_{p_\beta}(\omega)$ combine Equations (20), (29) and (31) and obtain

$$\frac{\partial \bar{\phi}^k_\alpha}{\partial x} + ik\bar{\phi}^k_\alpha = \sum_s D_{ks} \Delta C^s_{p_\alpha}(\omega) \tag{39}$$

where $\bar{\phi}^k_\alpha$ replaced ϕ^k_α in Equation (27). Hence, for known Mach number and reduced frequency, D_{ks} can be obtained from the equations in the previous section for a given wing geometry. The mode shape factor can be determined from structural calculations. With $\Delta C^s_{p_\alpha}$ known $S_{Q'_\alpha}(\omega)$ can be obtained from Equation (37), and hence the displacement and acceleration spectra.

3.0 RESULTS AND DISCUSSIONS

The steps involved in computing the response of the wing are fairly straightforward once the necessary aeroelastic data are given. As an example, the response of a F-4E wing is studied using structural and experimental data supplied by Mullans and Lemley (Ref. 11). Figure 6 is taken from Reference 11 and shows the choice of panel dimensions on the wing. A total of eighteen panels are used in the computations, and the panel centres are marked numerically from 1 to 18.

The first ten symmetrical and antisymmetric modes are considered in this example. The natural frequencies ω_{n_α}, generalized mass M_α, average mode shape $\vec{\phi}_\alpha^k$ and damping ratio ζ_α for three dynamic pressures Q = 220, 350 and 470 psf are tabulated in Mullans' and Lemley's report (Ref. 11). They also obtained buffet data from wind tunnel tests on a 10% scale rigid three-dimensional model. For a clean wing with zero leading edge and trailing edge deflections, the rms pressure coefficients $\Delta C_{p_{rms}}$ on the wing are shown in Figure 7. In this particular example, $\Delta C_{p_{rms}}$ varies practically linearly along both constant chord and constant span directions.

The power spectral densities of the pressure fluctuations at various points on the wing for Mach number 0.7 and angle of incidence 12° are also given in Reference 11. The transducers are not located exactly at the panel centres and there may be more than one transducer per panel or in some cases, none at all. Figure 8 indicates the transducers (numbers correspond to these given in Ref. 11) whose measured outputs are used to represent the fluctuating pressures on the panels where they are located.

Reference 11 also gives the mode shape $\vec{\phi}_\alpha^k$ for the symmetric and antisymmetric modes. To obtain $\frac{\partial \vec{\phi}_\alpha^k}{\partial x}$, a cubic spline algorithm is used in the present study. For given Mach number and reduced frequency, the normalwash factor D_{ks} in Equation (39) can be obtained using the analysis of Section 2.3. Upon substitution in Equation (38), Equation (37) can be solved for $S_{Q_\alpha'}(\omega)$ for known power spectrum of the external random load $S_{L_\alpha', D}(\omega)$. The spectra of the pressure fluctuations at each of the 18 panels are taken from Mullans and Lemley for q = 470 psf, M = 0.7 and $\alpha = 12°$. For other flow conditions, it is assumed that the spectra remain the same. Following Reference 2 the experimentally determined power spectral density curves from rigid model wind tunnel tests are expressed in series form and the coefficients in the series are obtained by a curve fitting procedure. Using proper scaling (Ref. 11) the pressure spectra at flight conditions can be obtained from wind tunnel tests.

The spectrum of the generalized force due to the random load, (Eq. (18)) can be calculated knowing the decay coefficients α and β and also the convection velocity U_c. Data for α and β from flight tests are extremely scarce. In order to show qualitatively the effect of a decaying pressure field and the difference in the response spectrum as compared to that for constant correlation assumption using Equation (16), the data from Coe et al. (Ref. 22) are used. It is assumed in this investigation that $\beta = \alpha$, and α is determined from measurements of surface pressure fluctuations in a turbulent boundary layer. The decay coefficient is expressed in the form

$$\alpha\delta = A\left(\frac{X}{X_0}\right)^B \tag{40}$$

where δ is the boundary layer thickness, A and B are constants and

$$X = \frac{f\delta}{U} \tag{41}$$

f is the frequency. From Reference 22 A and B are taken to be 0.2 and .3891 respectively for separated flow, and $X_0 = 0.001$. To calculate the boundary layer thickness, the formula given by Bies (Ref. 23) is used, that is,

$$\frac{\delta}{x} = 0.37\, R_{e_x}^{-1/5} \left[1 + \left(\frac{R_{e_x}}{6.9 \times 10^7} \right)^2 \right]^{1/10} \qquad (42)$$

The Reynolds Number R_{e_x} is calculated based on midspan chord. Taking x to be equal to the midspan chord. The value of δ thus calculated when substituted into Equation (40) gives an approximate average value for α which is assumed to be constant at all the panels. It is a function of Mach number, frequency and flight altitude only.

Figures 9 and 10 show a comparison of the response acceleration power spectral density from flight tests (Ref. 11) with theoretical predictions at M = 0.78, Q = 220 psf and M = 0.82, Q = 350 psf respectively. The location of the accelerometer is at 84% semispan and 26% chord. The constant correlation assumption using Equation (16) for the input load is applied to all the panels. Two sets of damping values are used: a structural damping ratio of 0.05 for all modes, and damping ratios determined experimentally from flight tests (Ref. 11). The ten symmetric and antisymmetric modes have been considered in the computations. It is seen from these two figures that at low frequencies below 25 Hz the theoretical predictions are fairly good. However, at higher frequencies, the predicted values are nearly tenfold the experimental flight test results.

The effect of altitude and Mach number on the acceleration and displacement spectra at constant dynamic pressure Q are shown in Figures 11 to 14 for an assumed value of 0.05 for the structural damping ratio. At Q = 220 psf, the response at low frequencies does not depend too strongly on Mach number and altitude, while at the higher frequency range of the spectra the effect of Mach number can be seen. It is of interest to note from these figures that the response decreases for increasing Mach number and altitude at low frequencies around 10 Hz while at higher frequencies the reverse is true.

Figures 15 to 18 show the response at two Mach numbers M = 0.51 and 0.78 for various values of Q and altitude. They all show that the response is strongly dependent on Q. Dividing the response by Q^2, Figures 19 and 20 show that the curves can roughly be collapsed into a single curve indicating a Q^2 dependence. However, at M = 0.78, a similar behaviour is not observed.

At constant altitude of 15,000 ft., the variation of the response with Mach number and Q are shown in Figures 23 and 24. As expected, the response increases with Mach number and Q throughout the whole frequency spectrum. The effect of varying the structural damping is shown in Figures 25 to 28 for M = 0.78, Q = 220 psf and M = 0.82, Q = 350 respectively.

To obtain better agreement between theoretical and experimental results than those shown in Figures 9 and 10 at the higher frequencies, Equation (18) is used to represent the input load spectrum using values of decay coefficients derived from Equations (40) to (42) and a value of the convection velocity $U_c = 0.80U$. These results are shown in Figures 29 to 32. From the acceleration spectra at M = 0.78 and 0.82 (Figs. 29 and 31), it can be seen that the high frequency range of the spectra has been much improved and agrees well with flight test data. However, at low frequencies, the constant correlation assumption seems to give better agreement. This is probably due to the inaccuracies of the decay coefficients obtained by extrapolation of data obtained at much higher frequencies.

Figures 33 and 34 also show comparisons between flight test data and theoretical predictions. These figures are prepared by combining Figures 9 and 10 with Figures 29 and 31 for M = 0.78, Q = 270 psf and M = 0.82, Q = 350 psf respectively. The predictions from Reference 11 which considered only the structural response are also included to show the effect of unsteady aerodynamics in the response calculations. At low frequencies below 15 Hz, improvements over predictions which considered only the structural dynamics of the wing are quite noticeable. However, at the higher frequency range of the spectra, unsteady aerodynamic effects become less important.

4.0 CONCLUSIONS

A panel method for predicting the acceleration and displacement response of a wing to random loading has been developed taking into consideration the coupling between the structural dynamics and aerodynamics of a vibrating wing. The doublet-lattice method is found to be most suitable in the present panelling scheme to compute the unsteady aerodynamic forces.

Using available structural data for the F-4E wing together with rigid model wind tunnel fluctuating pressure measurements, the displacement and acceleration response have been computed for various Mach numbers, dynamic pressures and flight altitudes. The results indicate that the response is most affected by changes in dynamic pressure and Mach number.

At low frequencies, improvements in the response predictions over those which considered only the structural dynamics but excluded the unsteady aerodynamic forces generated by the vibrating wing are quite significant. However, at the higher frequency range of the spectra, unsteady aerodynamic effects become less important.

Two methods have been used to represent the spectrum of the input random load. Using the constant correlation assumption, comparison of the computed acceleration power spectra with those from flight tests shows that at low frequencies the agreement is fairly good, but at high frequencies, the predicted values are nearly tenfolds the experimental results. Much better agreement at the higher frequencies is obtained when the exponential spatially decaying form of the cross-power spectral density for the fluctuating pressures is used. However, this results in discrepancies at low frequencies which are probably due to the extrapolation of the decay coefficients from data obtained at much higher frequencies. The results illustrate the importance of a proper representation of the input load spectrum.

5.0 REFERENCES

1. Lee, B.H.K. — *Theoretical Analysis of the Transient Response of a Wing to Non-Stationary Buffet Loads.* NRC, NAE Aero. Rept. LR-597, National Research Council Canada, April 1979.

2. Lee, B.H.K. — *A Method for the Prediction of Wing Response to Non-Stationary Buffet Loads.* NRC, NAE Aero. Rept. LR-601, National Research Council Canada, July 1980.

3. Liepman, H.W. — *On the Application of Statistical Concepts to the Buffeting Problems.* Journal Aeronautical Sciences, Vol. 19, No. 12, December 1952, pp. 793-800.

4. Liepman, H.W. — *Extension of the Statistical Approach to Buffeting and Gust Response of Wings of Finite Span.* Journal Aeronautical Sciences, Vol. 22, No. 3, March 1955, pp. 197-200.

5. Ribner, H.S. — *Spectral Theory of Buffeting and Gust Response: Unification and Extension.* Journal Aeronautical Sciences, Vol. 23, No. 12, December 1956, pp. 1075-1077.

6. Huston, W.B.
Skopinski, T.H. — *Measurement of Analysis of Wing and Tail Buffeting Loads in a Fighter Airplane.* National Advisory Committee for Aeronautics, Report 1219, 1955.

7. Huston, W.B.
Skopinski, T.H.
Probability and Frequency Characteristics of Some Flight Buffet Loads.
National Advisory Committee for Aeronautics, Technical Note 3733, 1956.

8. Huston, W.B.
A Study of the Correlation Between Flight and Wind Tunnel Buffet Loads.
North Atlantic Treaty Organization for Aeronautical Research and Development, Report 111, April-May 1957.

9. Skopinski, T.H.
Huston, W.B.
A Semi-Empirical Procedure for Estimating Wing Buffet Loads in the Transonic Region.
National Advisory Committee for Aeronautics, RML56E01, September 1956.

10. Davis, D.D.
Wornom, D.E.
Buffet Tests of an Attack-Airplane Model with Emphasis on Analysis of Data from Wind-Tunnel Tests.
National Advisory Committee for Aeronautics, RML57H13, February 1958.

11. Mullans, R.E.
Lemley, C.E.
Buffet Dynamic Loads during Transonic Maneuvers.
Air Force Flight Dynamics Laboratory Technical Report AFFDL-TR-72-46, September 1972.

12. Hwang, C.
Pi, W.S.
Transonic Buffet Behaviour of Northrop F-5A Aircraft.
American Institute of Aeronautics and Astronautics, Paper 75-70, January 1975.

13. Hwang, C.
Pi, W.S.
Investigation of Steady and Fluctuating Pressure Associated with the Transonic Buffeting and Wing Rock of a One-Seventh Scale Model of the F-5A Aircraft.
National Aeronautical and Space Administration, CR-3061, November 1978.

14. Jones, J.G.
A Survey of the Dynamic Analysis of Buffeting and Related Phenomenon.
Royal Aircraft Establishment Technical Report 72197, February 1973.

15. Butler, G.F.
Spavins, G.R.
Preliminary Evaluation of a Technique for Predicting Buffet Loads in Flight from Wind-Tunnel Measurements on Models of Conventional Construction.
North Atlantic Treaty Organisation, Advisory Group for Aerospace Research and Development, Paper 23 of AGARD CP-204, 1976.

16. Schweiker, J.W.
Davis, R.E.
Response of Complex Shell Structures to Aerodynamic Noise.
National Aeronautics and Space Administration, CR-450, April 1966.

17. Rodden, W.P.
Giesing, J.P.
Kalman, T.P.
Refinement of the Nonplanar Subsonic Doublet-Lattice Lifting Surface Method.
J. Aircraft, Vol. 9, No. 1, January 1972, pp. 69-73.

18. Kalman, T.P.
Rodden, W.P.
Giesing, J.P.
Application of the Doublet-Lattice Method to Nonplanar Configurations in Subsonic Flow.
J. Aircraft, Vol. 8, No. 6, June 1971, pp. 406-413.

19. Rodden, W.P.
Giesing, J.P.
Kalman, T.P.
New Developments and Applications of the Subsonic Doublet-Lattice Method for Nonplanar Configurations.
Symposium on Unsteady Aerodynamics for Aeroelastic Analyses of Interfering Surfaces. North Atlantic Treaty Organization, Advisory Group for Aerospace Research and Development, AGARD-CP-80-71, 1971.

20. Landahl, M.T. *Kernel Function for Nonplanar Oscillating Surfaces in Subsonic Flow.* AIAA Journal, Vol. 5, No. 5, May 1967, pp. 1045-1046.

21. Hedman, S.G. *Vortex Lattice Method for Calculation of Quasi Steady State Loadings on Thin Elastic Wings in Subsonic Flow.* Aeronautical Research Institute of Sweden, Stockholm, Report 105, October 1965.

22. Coe, C.F.
Chyu, W.J.
Dods, J.B., Jr. *Pressure Fluctuations Underlying Attached and Separated Supersonic Turbulent Boundary Layers and Shock Waves.* AIAA Paper 73-996, October 1973.

23. Bies, D.A. *Review of Flight and Wind Tunnel Measurements of Boundary Layer Pressure Fluctuations and Induced Structural Response.* National Aeronautical and Space Administration, NASA CR-626, October 1966.

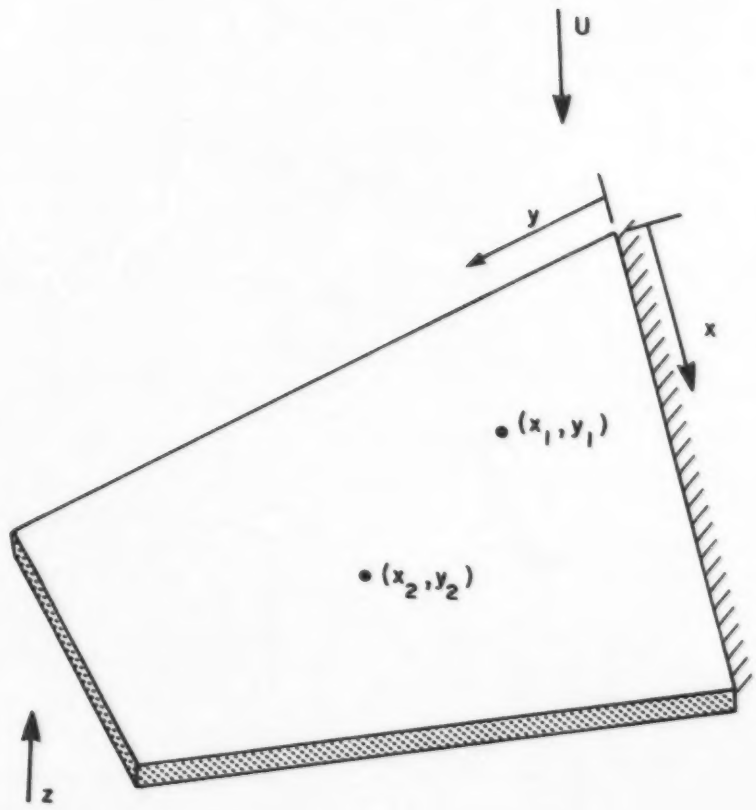

FIG. 1: SCHEMATIC OF WING

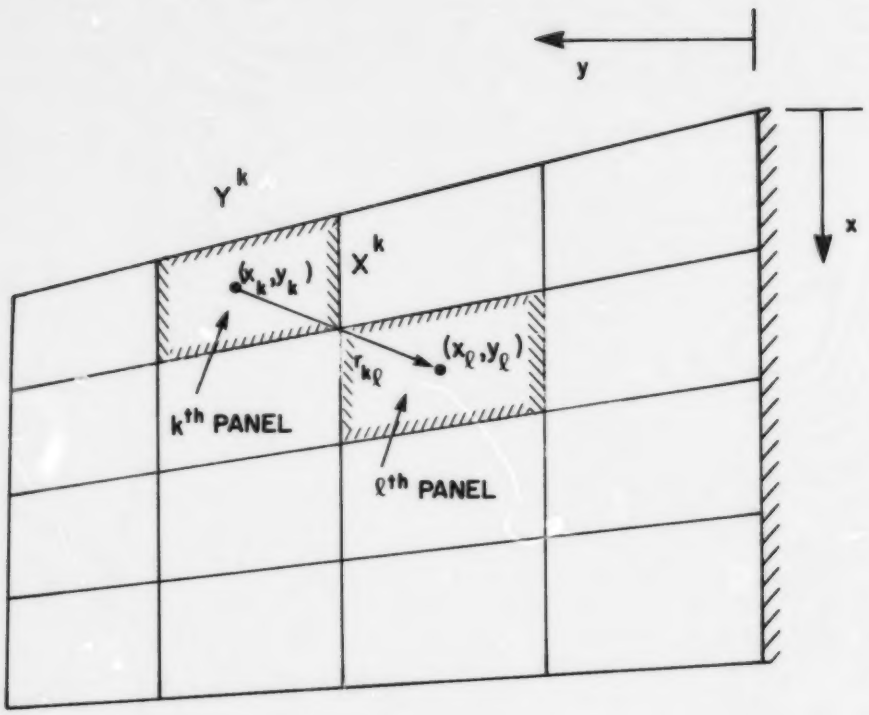

FIG. 2: PANEL REPRESENTATION OF WING

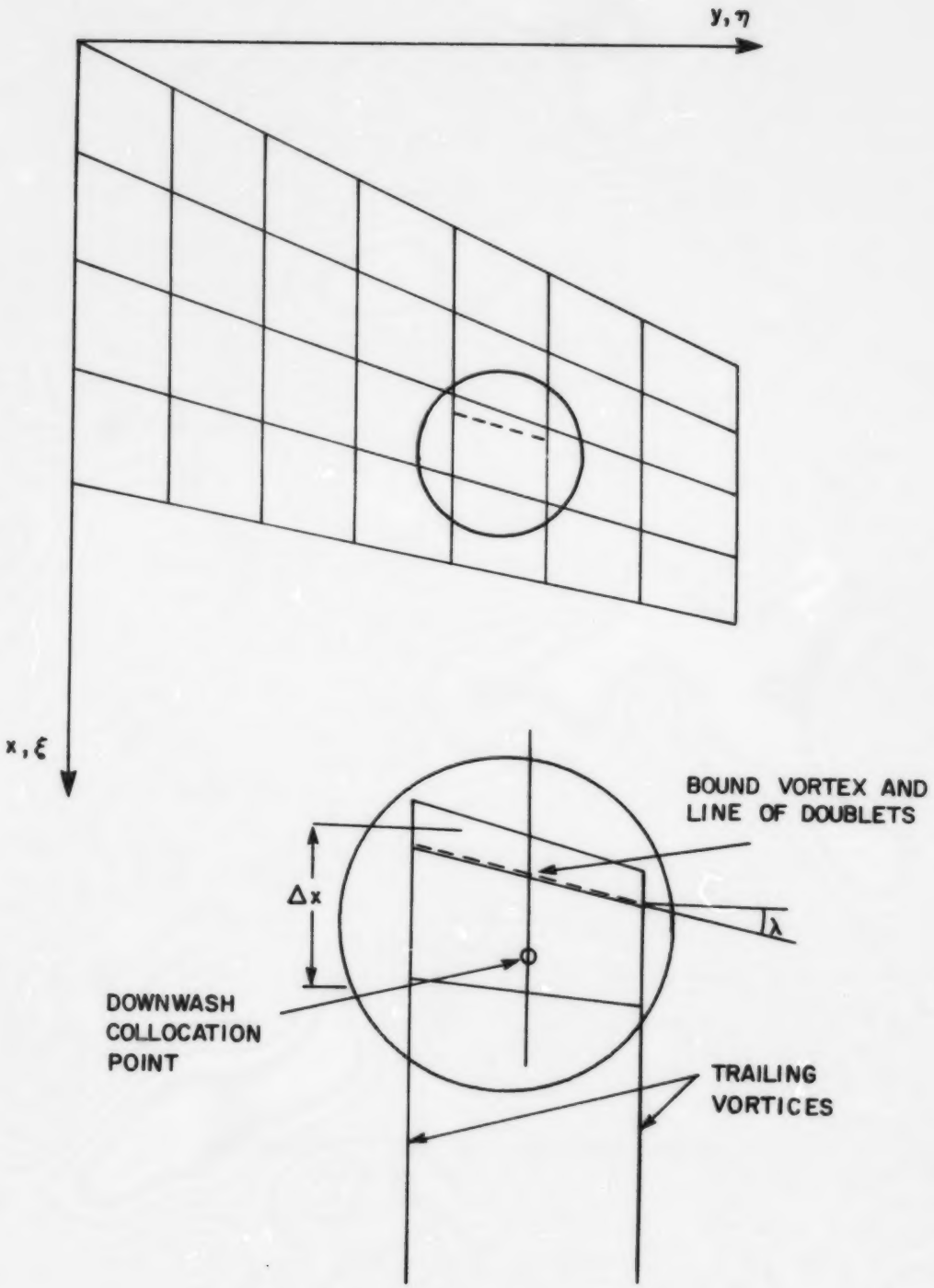

FIG. 3: REPRESENTATION OF WING BY PANELS AND LOCATION OF VORTICES, DOUBLETS AND COLLOCATION POINTS

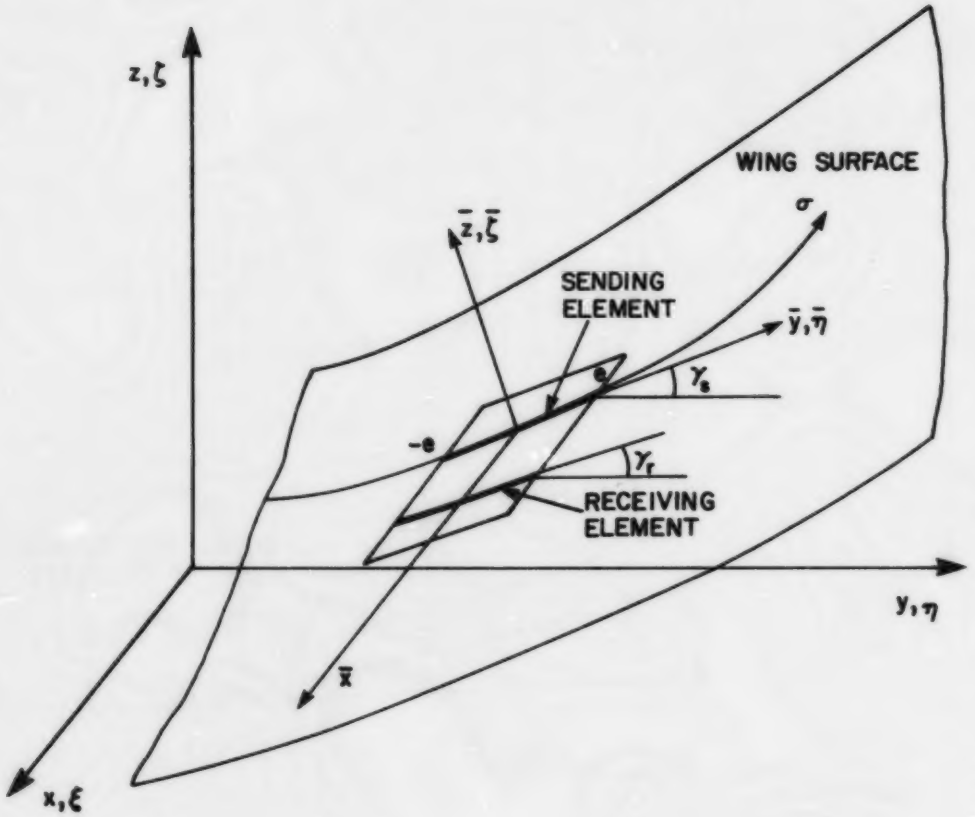

FIG. 4: WING AND ELEMENT CO-ORDINATES

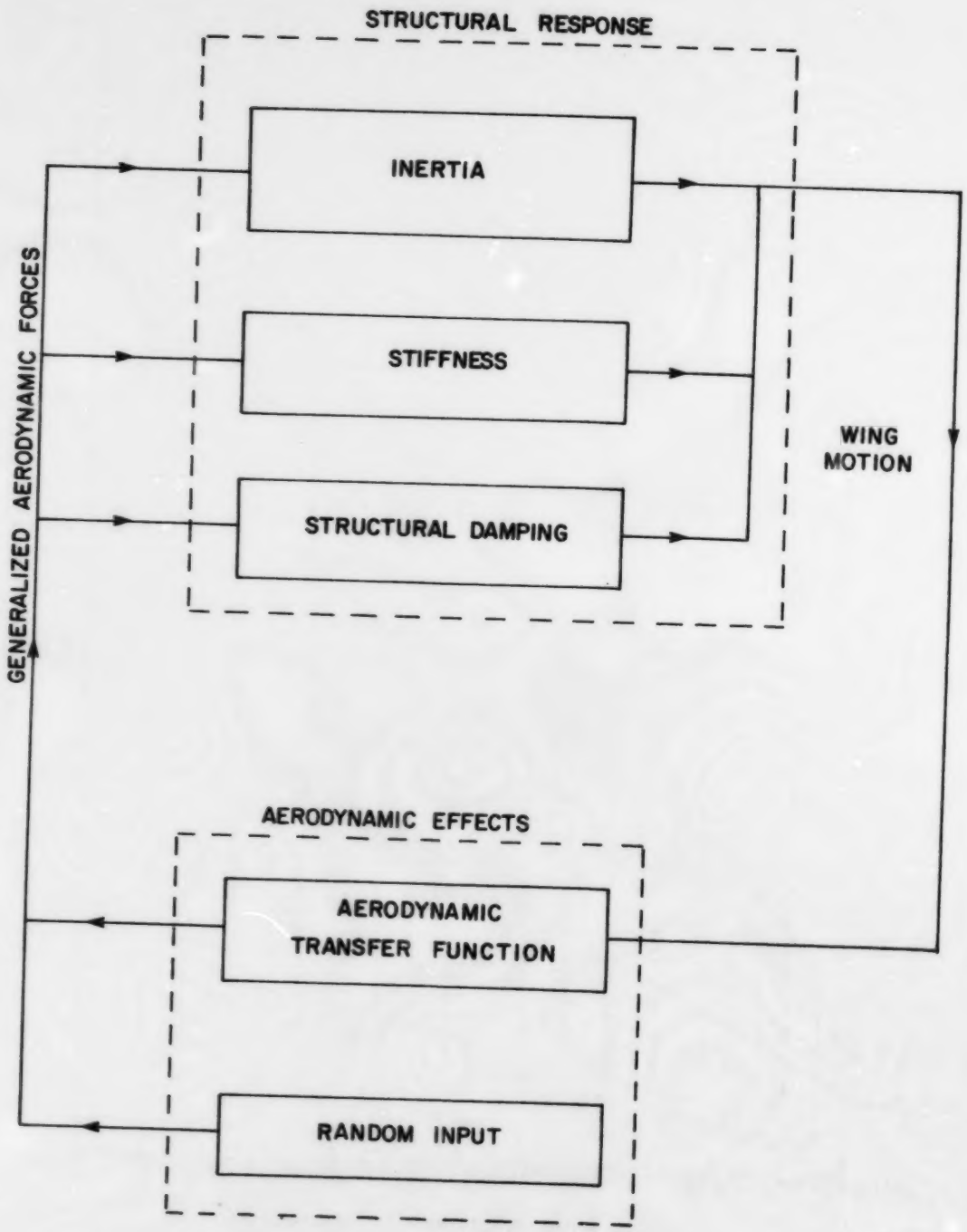

FIG. 5: BLOCK DIAGRAM FOR WING RESPONSE TO RANDOM LOADING

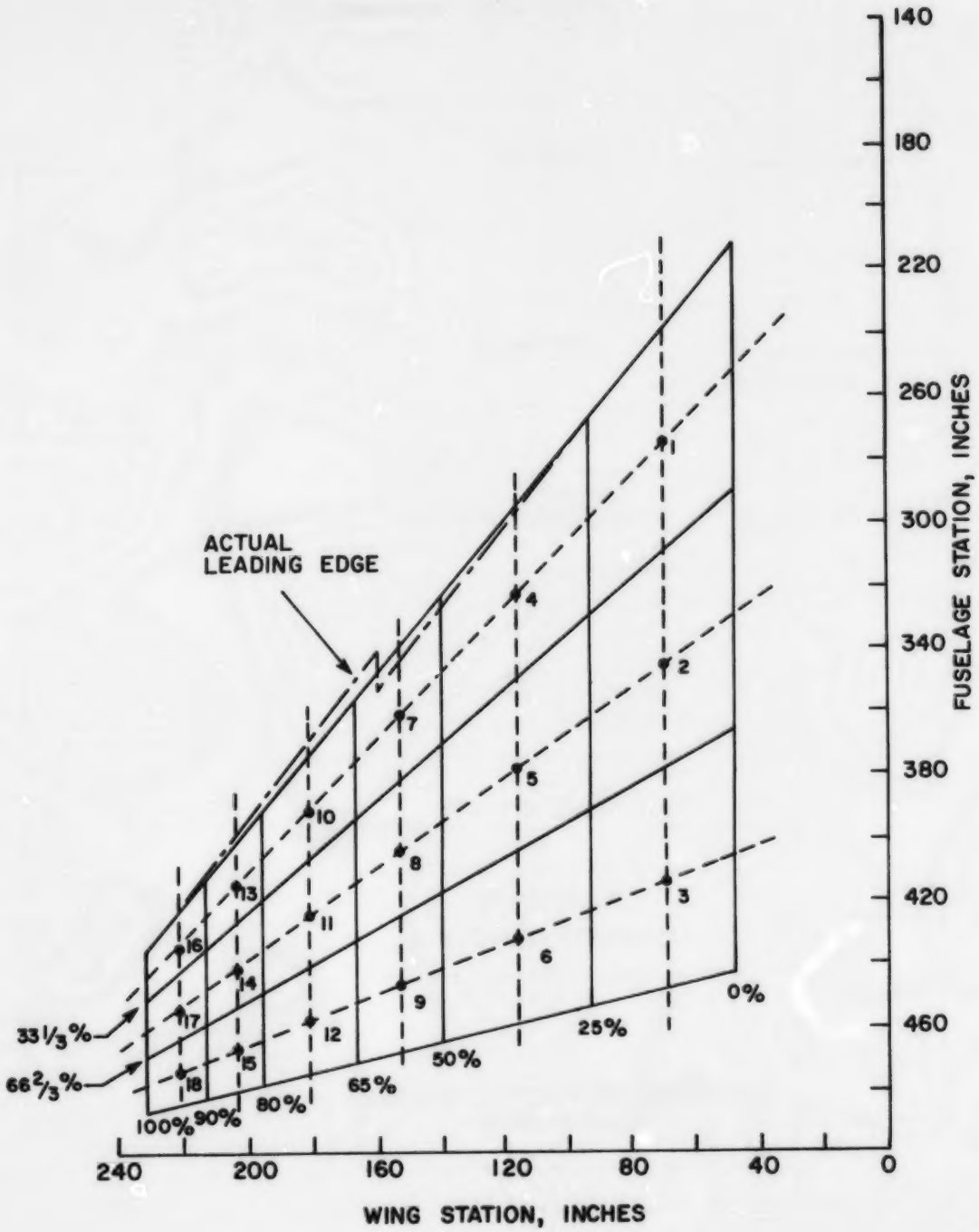

FIG. 6: PANEL REPRESENTATION OF F-4E WING PLANFORM

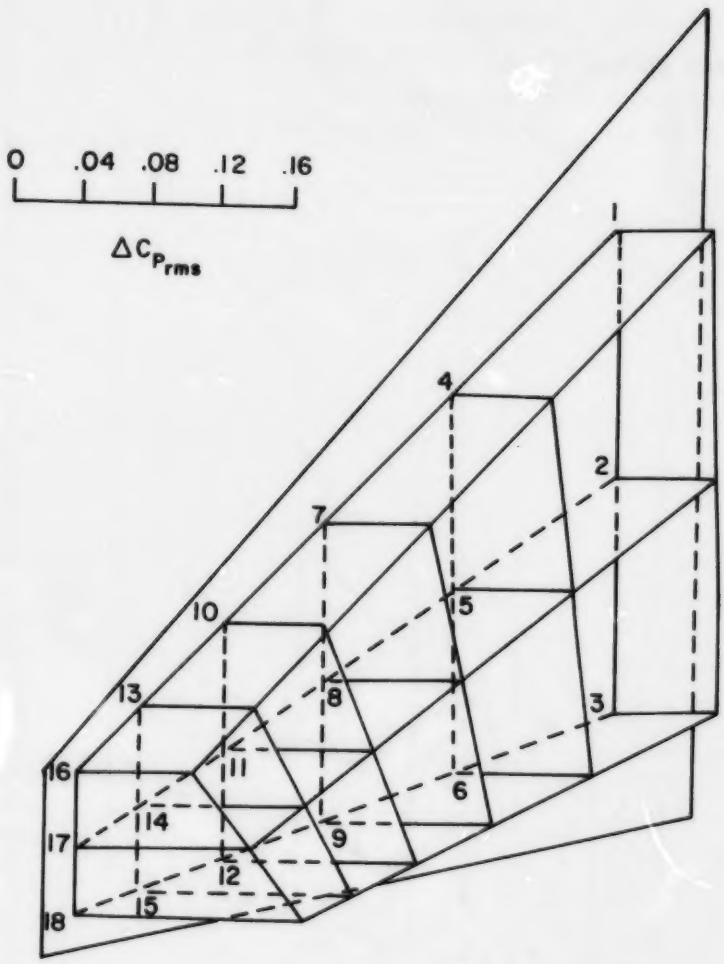

FIG. 7: APPROXIMATE MODELLING OF RMS PRESSURE COEFFICIENT ON WING

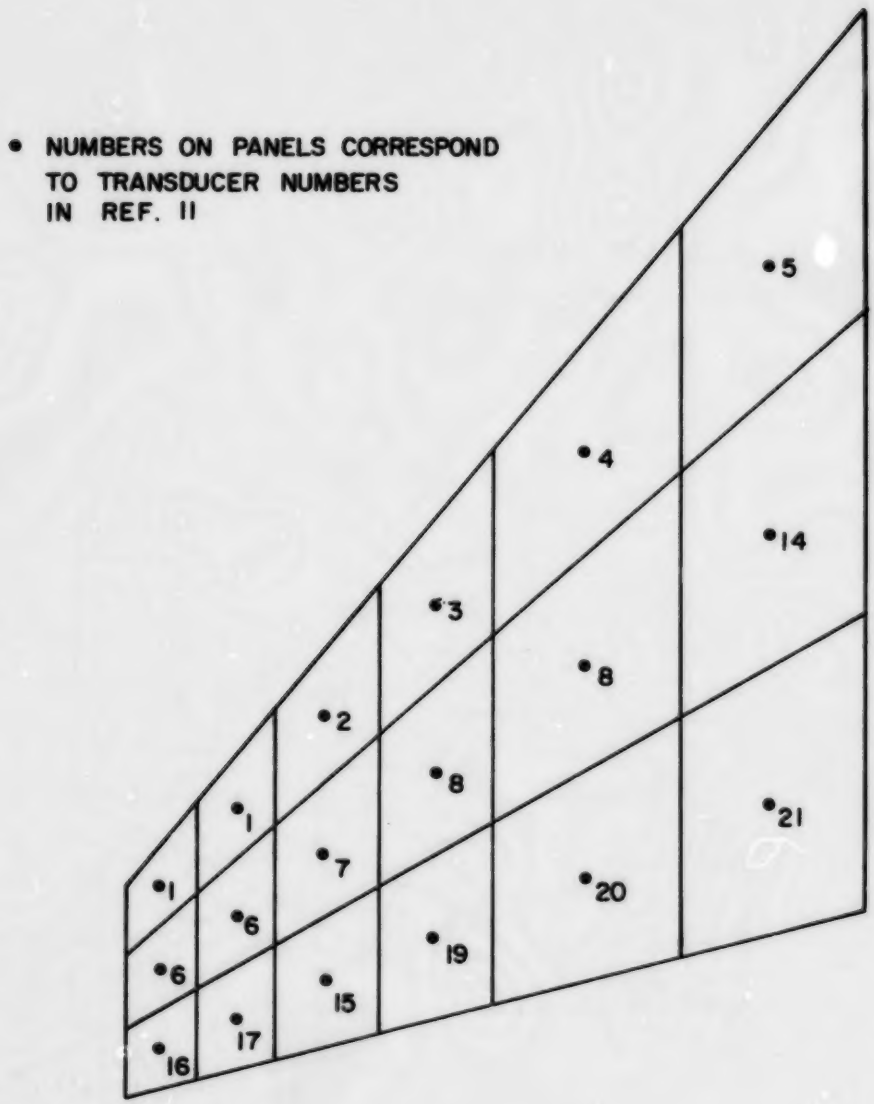

FIG. 8: PRESSURE TRANSDUCER LOCATIONS

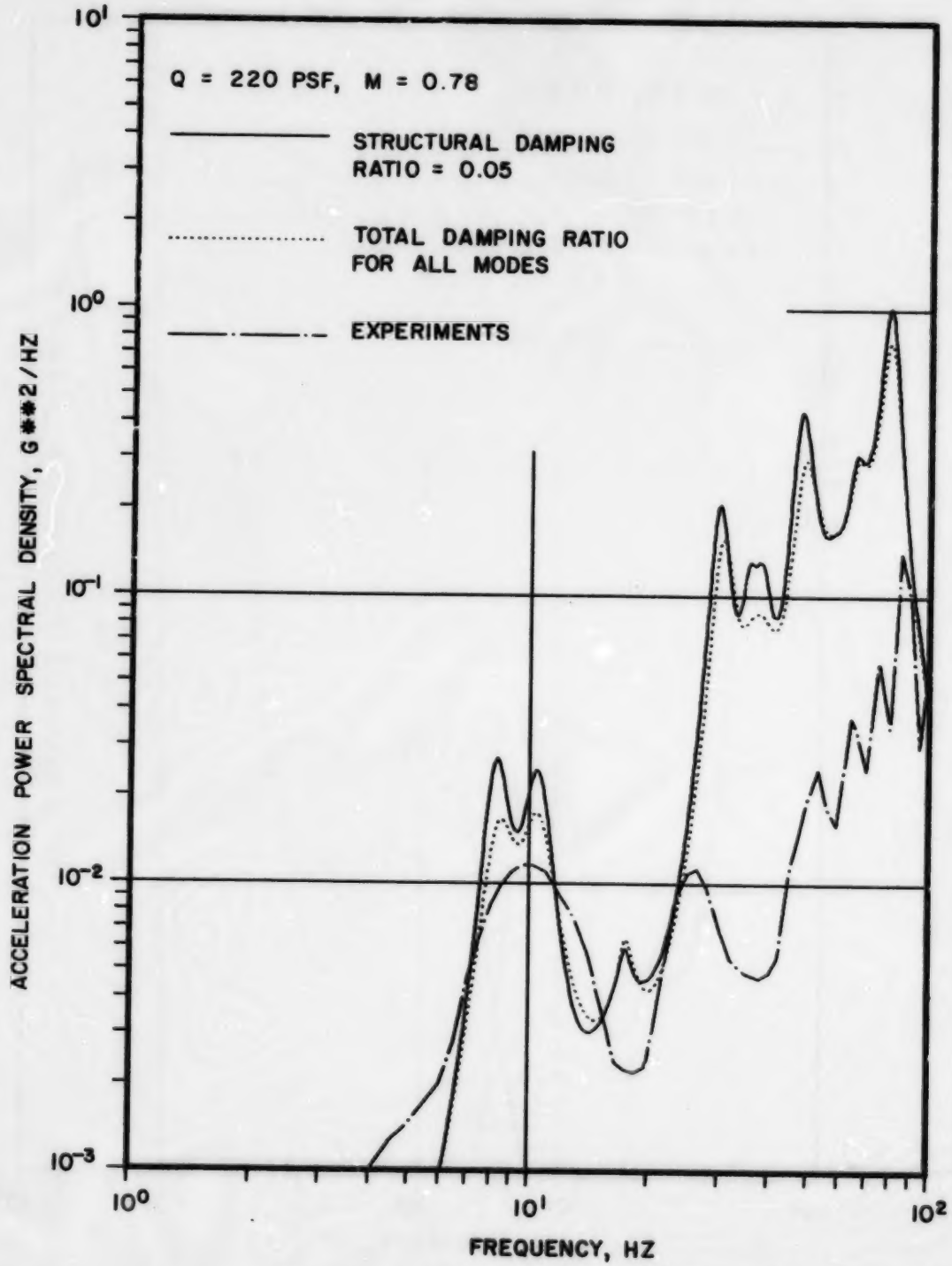

FIG. 9: COMPARISON OF RESPONSE ACCELERATION POWER SPECTRAL DENSITY FROM FLIGHT TESTS WITH THEORETICAL PREDICTIONS USING CONSTANT CORRELATION ASSUMPTION AT M = 0.78 AND Q = 220 PSF

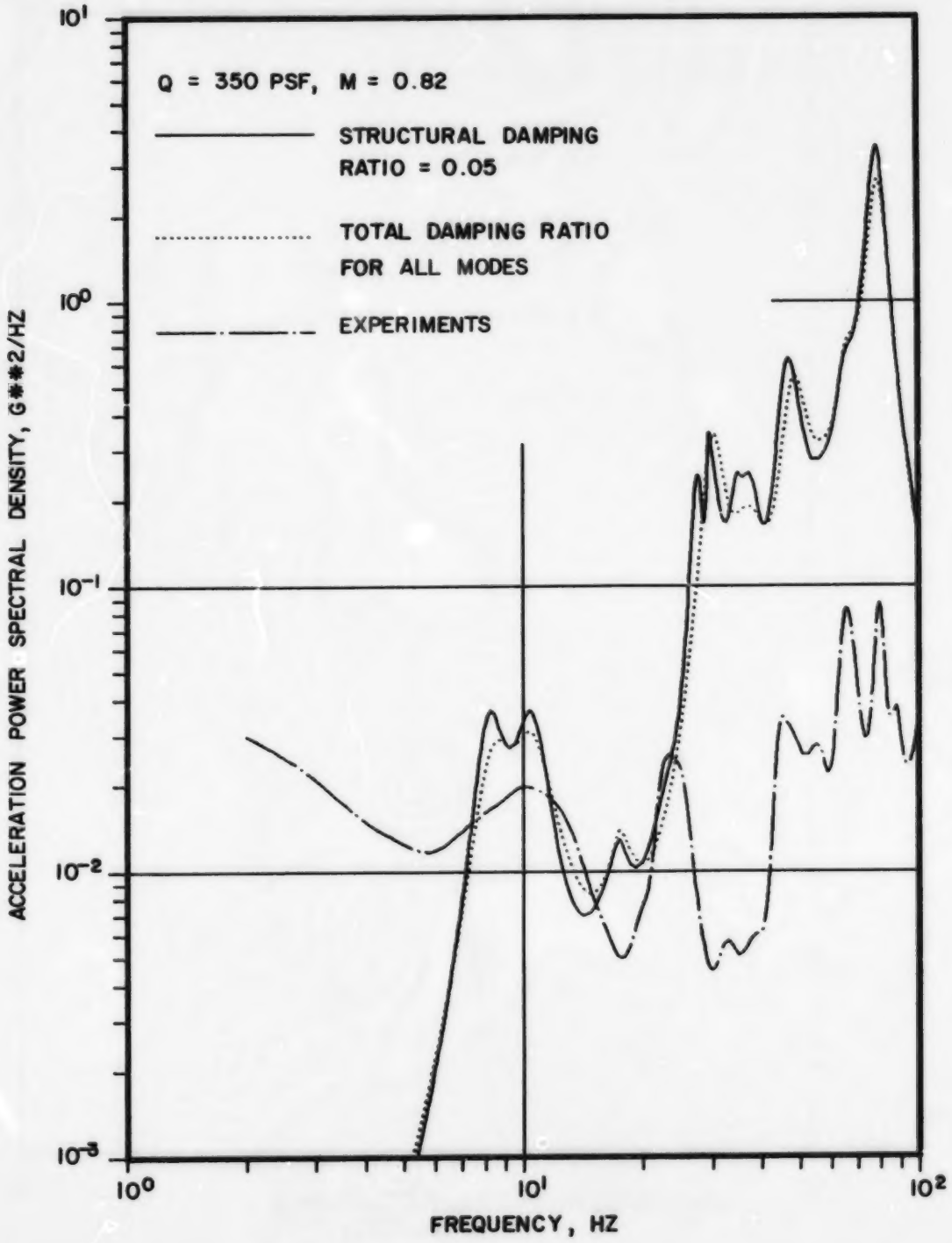

FIG. 10: COMPARISON OF RESPONSE ACCELERATION POWER SPECTRAL DENSITY FROM FLIGHT TESTS WITH THEORETICAL PREDICTIONS USING CONSTANT CORRELATION ASSUMPTION AT M = 0.82 AND Q = 350 PSF

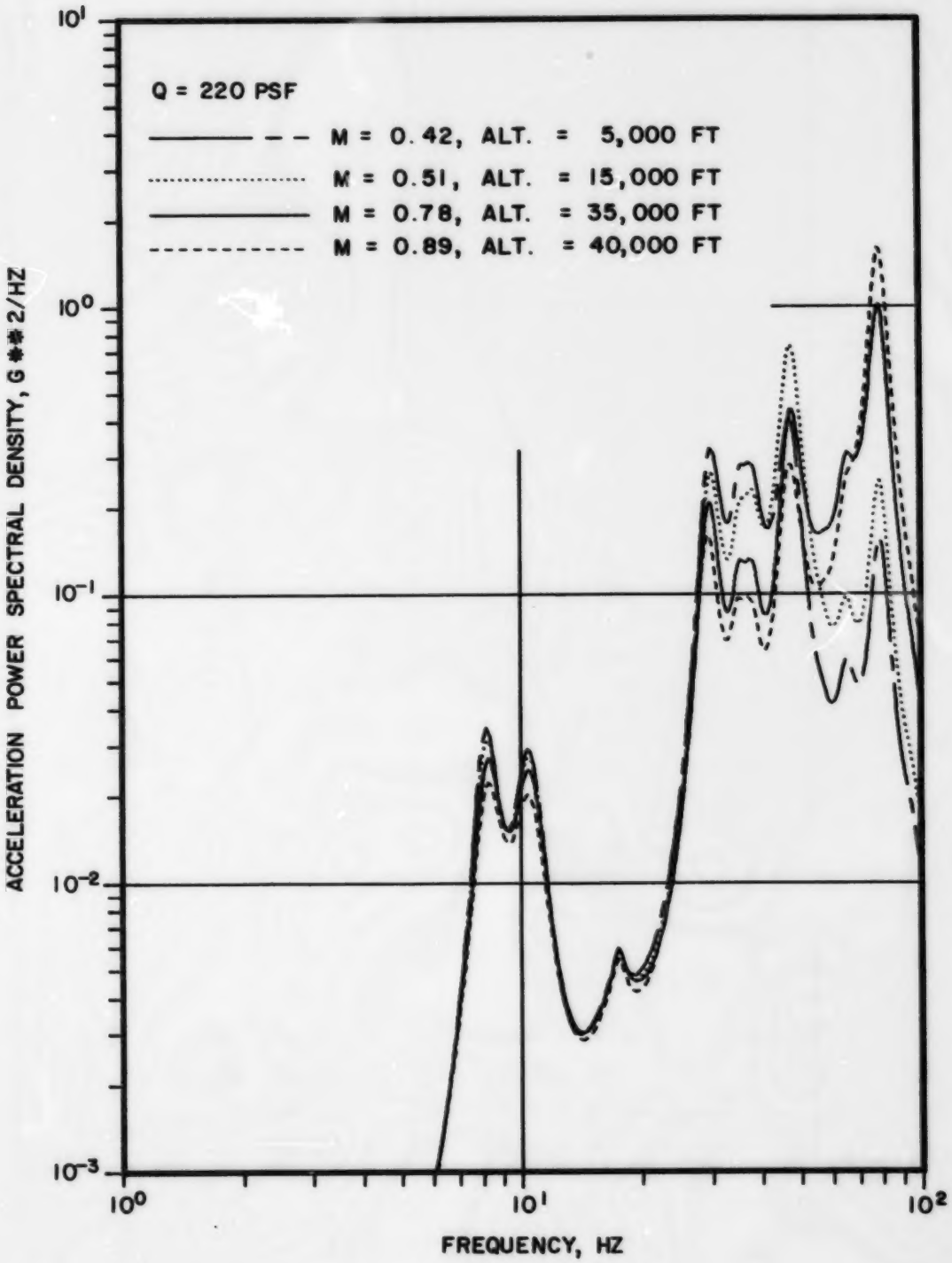

FIG. 11: VARIATION OF ACCELERATION POWER SPECTRAL DENSITY WITH MACH NUMBER AND FLIGHT ALTITUDE FOR Q = 220 PSF

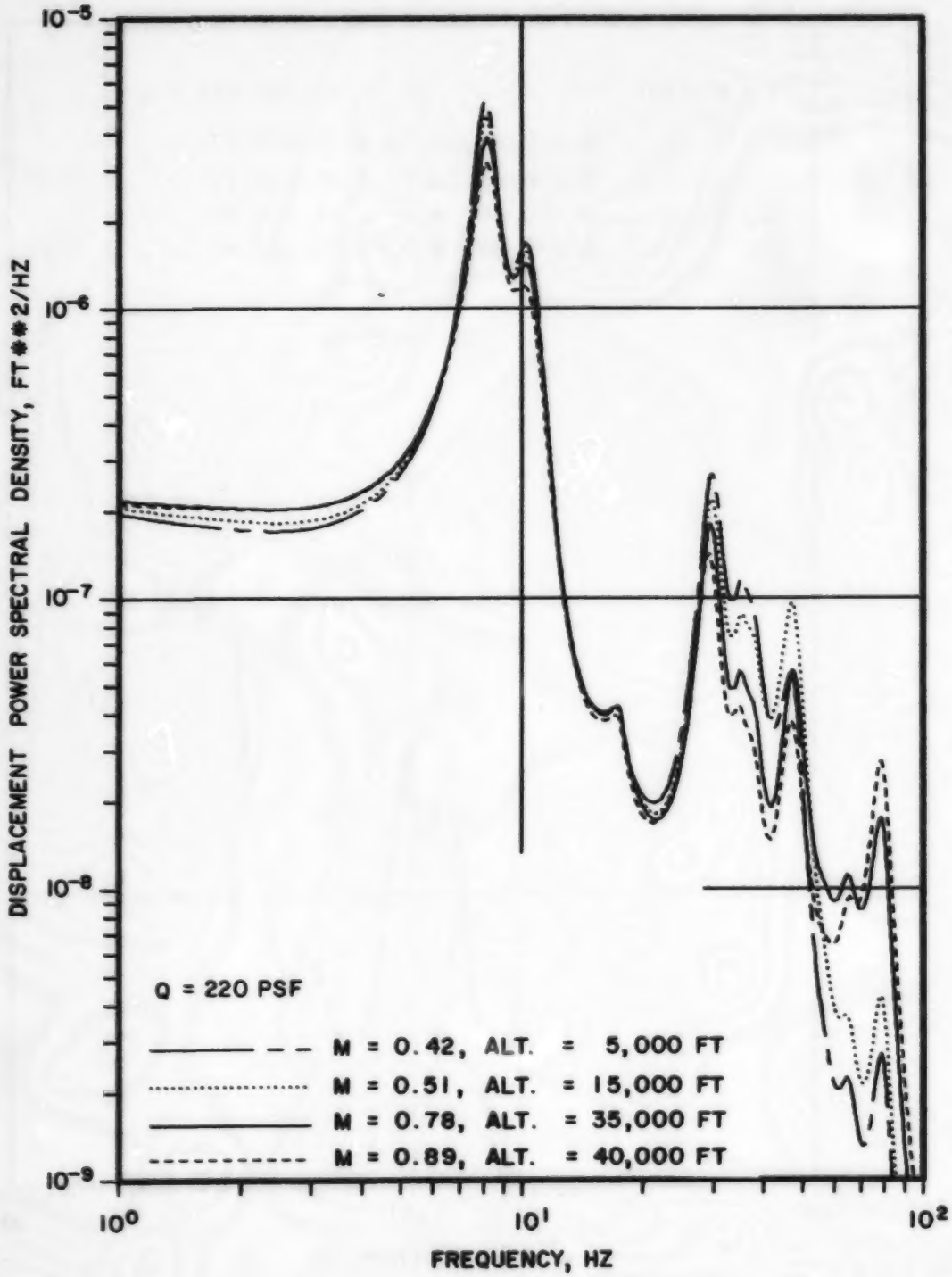

FIG. 12: VARIATION OF DISPLACEMENT POWER SPECTRAL DENSITY WITH MACH NUMBER AND FLIGHT ALTITUDE FOR Q = 220 PSF

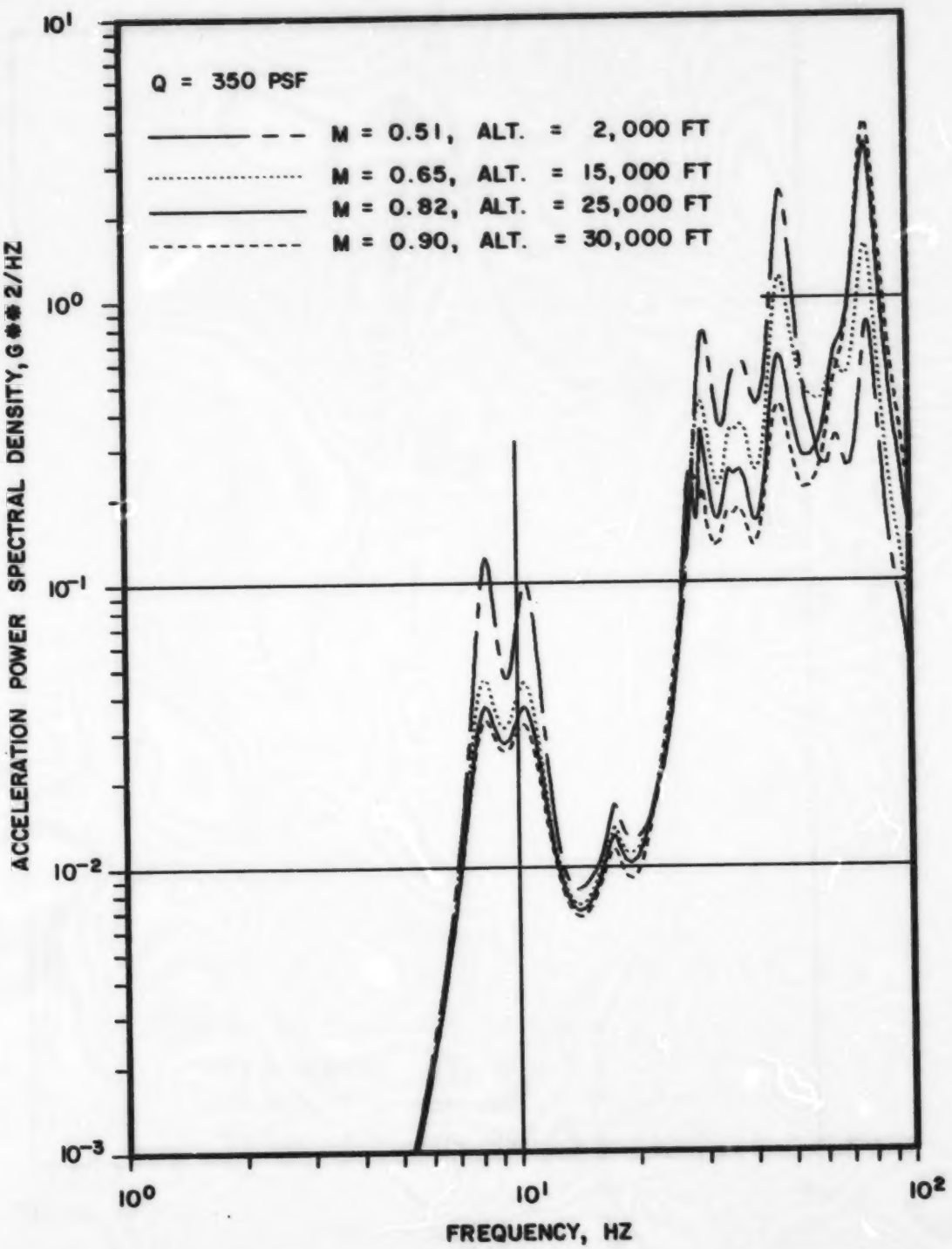

FIG. 13: VARIATION OF ACCELERATION POWER SPECTRAL DENSITY WITH MACH NUMBER AND FLIGHT ALTITUDE FOR Q = 350 PSF

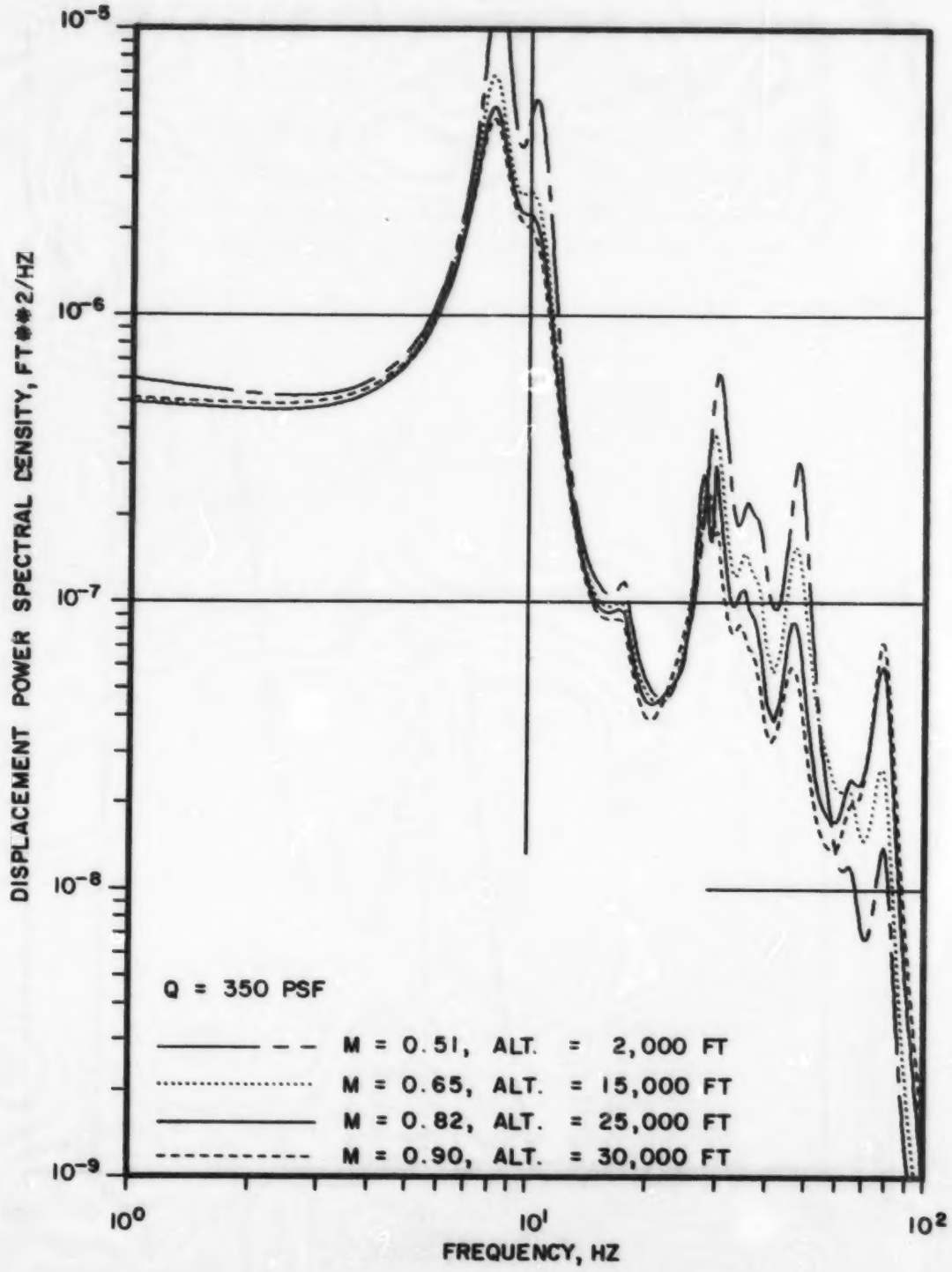

FIG. 14: VARIATION OF DISPLACEMENT POWER SPECTRAL DENSITY WITH MACH NUMBER AND FLIGHT ALTITUDE FOR Q = 350 PSF

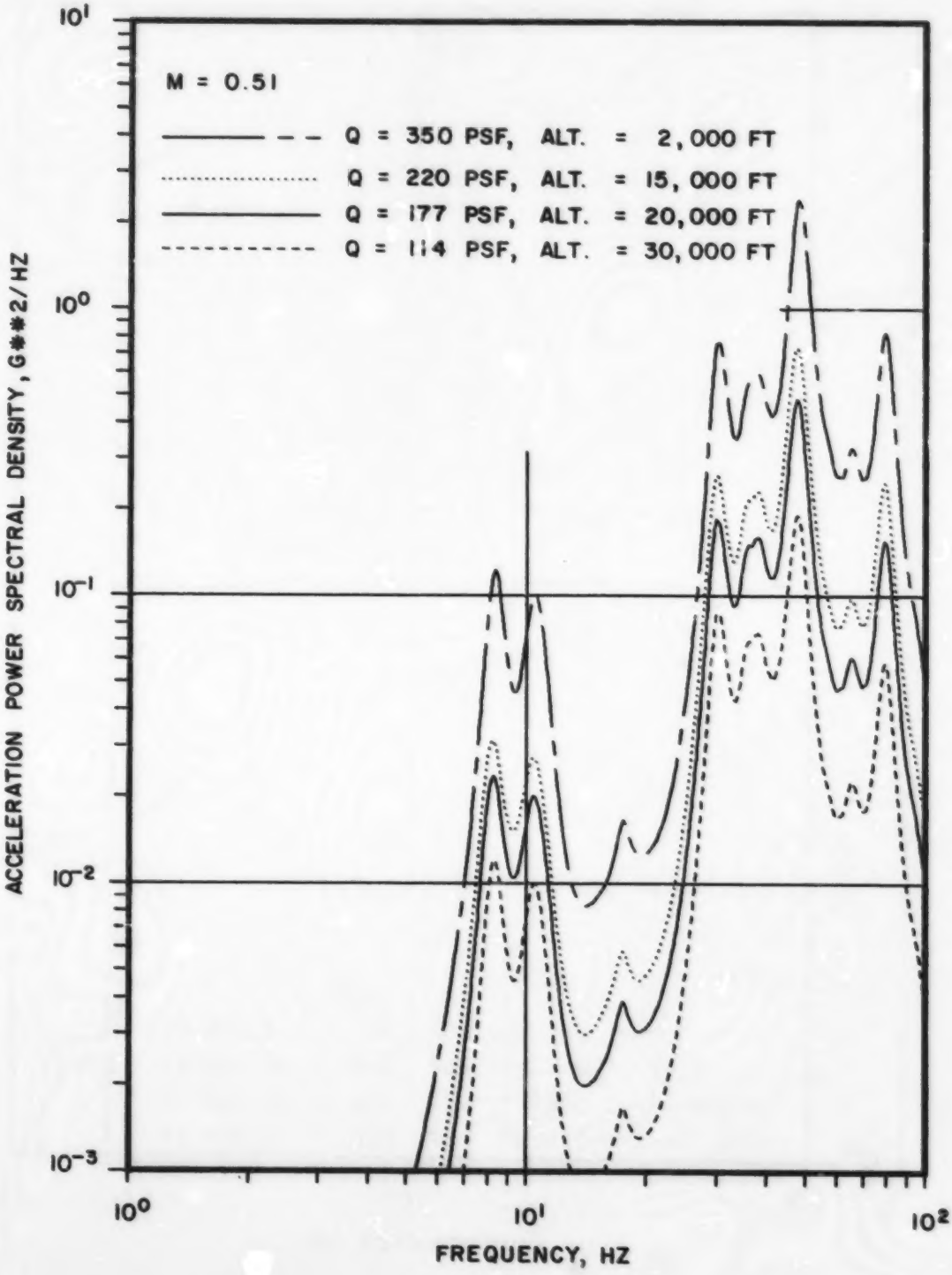

FIG. 15: VARIATION OF ACCELERATION POWER SPECTRAL DENSITY WITH DYNAMIC PRESSURE AND FLIGHT ALTITUDE FOR M = 0.51

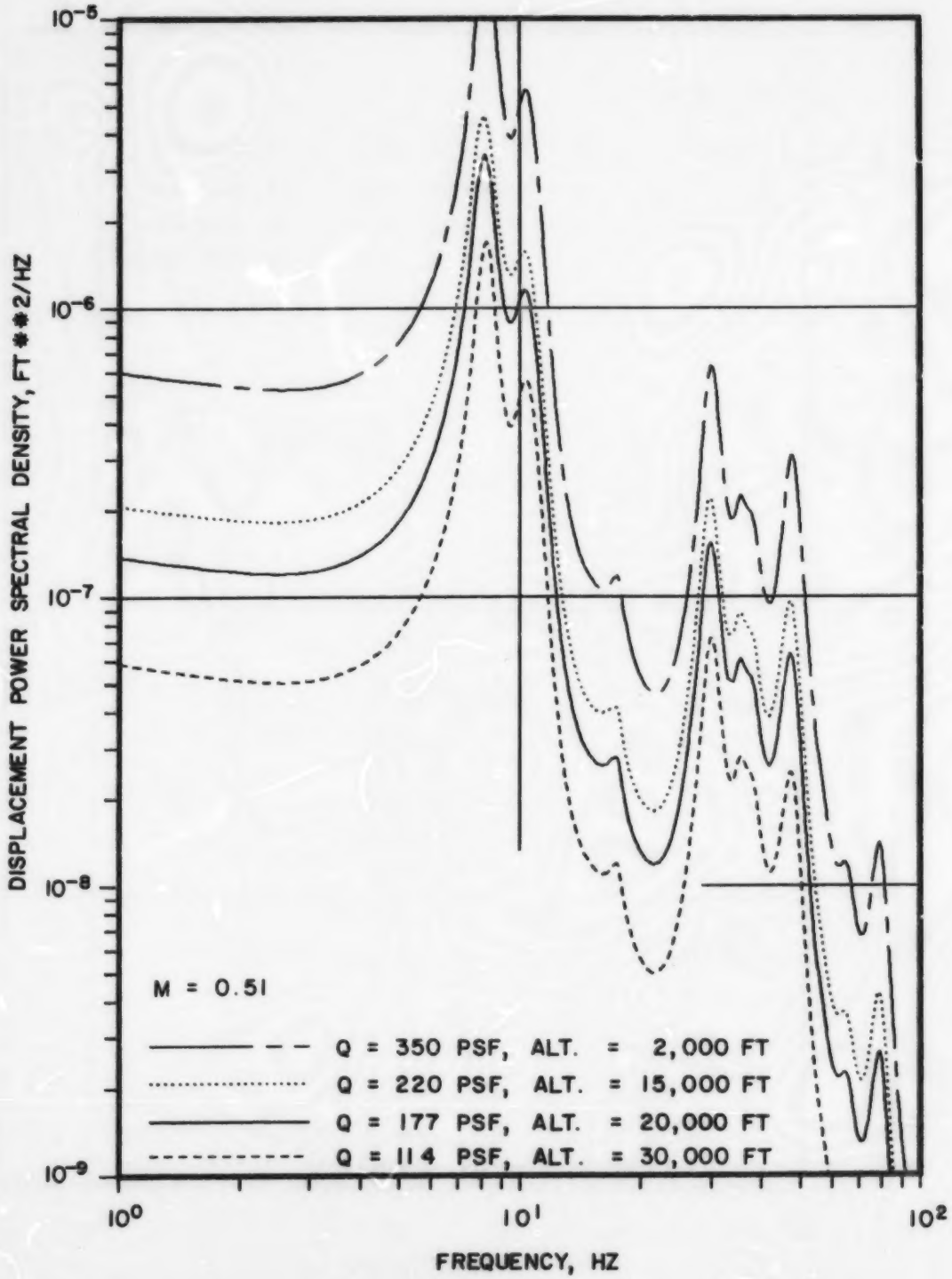

FIG. 16: VARIATION OF DISPLACEMENT POWER SPECTRAL DENSITY WITH DYNAMIC PRESSURE AND FLIGHT ALTITUDE FOR M = 0.51

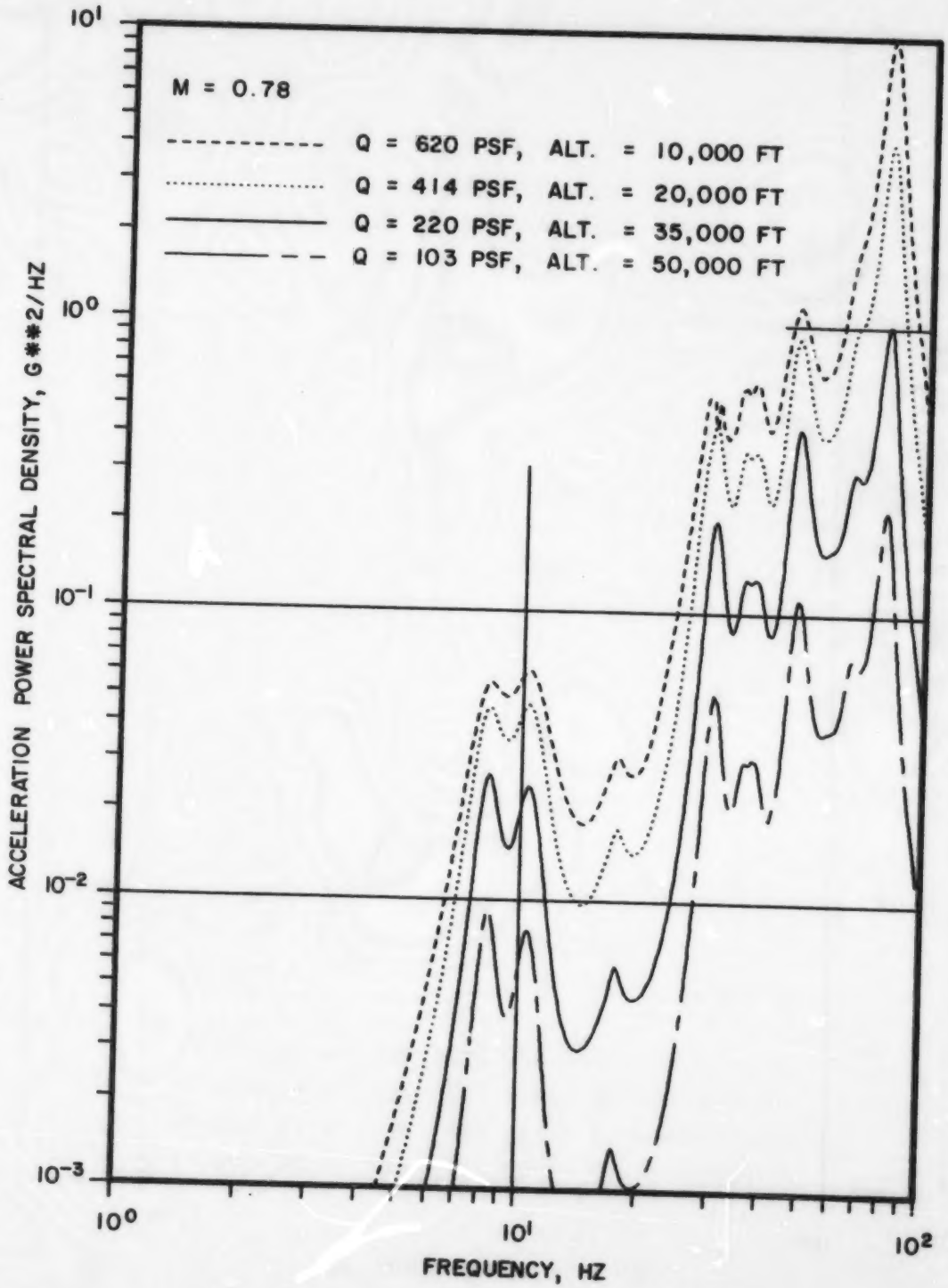

FIG. 17: VARIATION OF ACCELERATION POWER SPECTRAL DENSITY WITH DYNAMIC PRESSURE AND FLIGHT ALTITUDE FOR M = 0.78

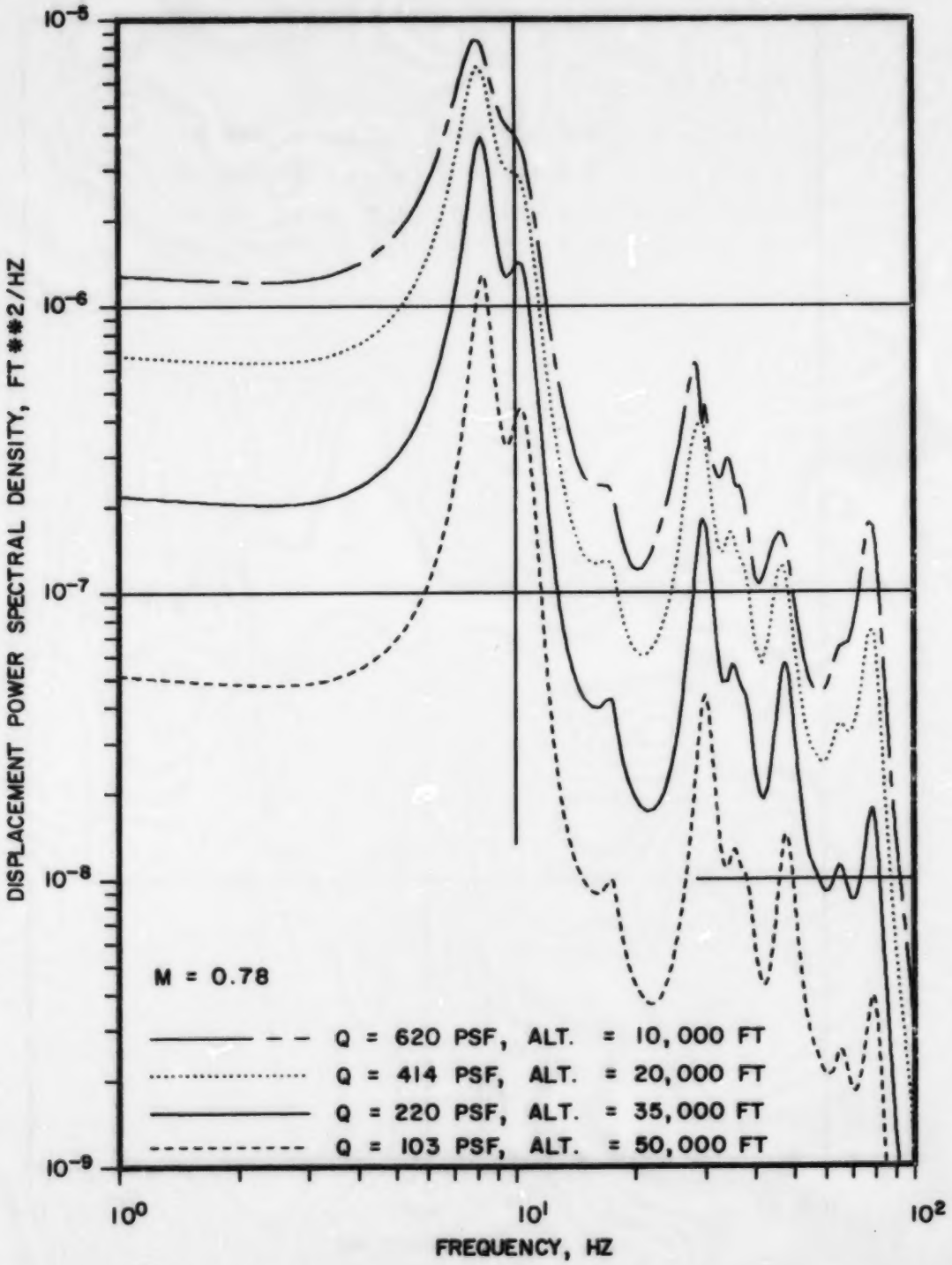

FIG. 18: VARIATION OF DISPLACEMENT POWER SPECTRAL DENSITY WITH DYNAMIC PRESSURE AND FLIGHT ALTITUDE FOR M = 0.78

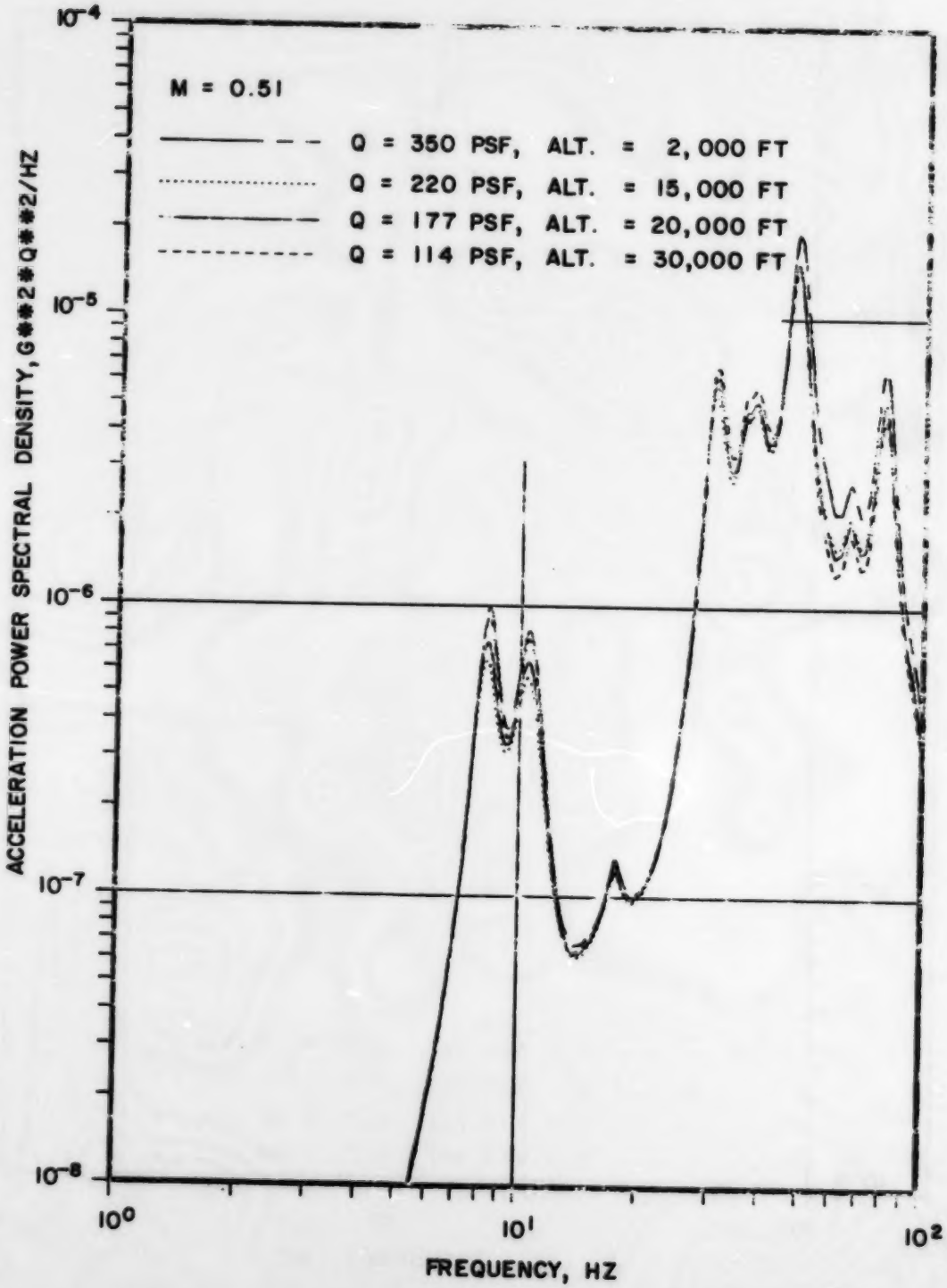

FIG. 19: VARIATION OF ACCELERATION POWER SPECTRAL DENSITY NORMALIZED WITH RESPECT TO Q^2 WITH DYNAMIC PRESSURE AND FLIGHT ALTITUDE FOR M = 0.51

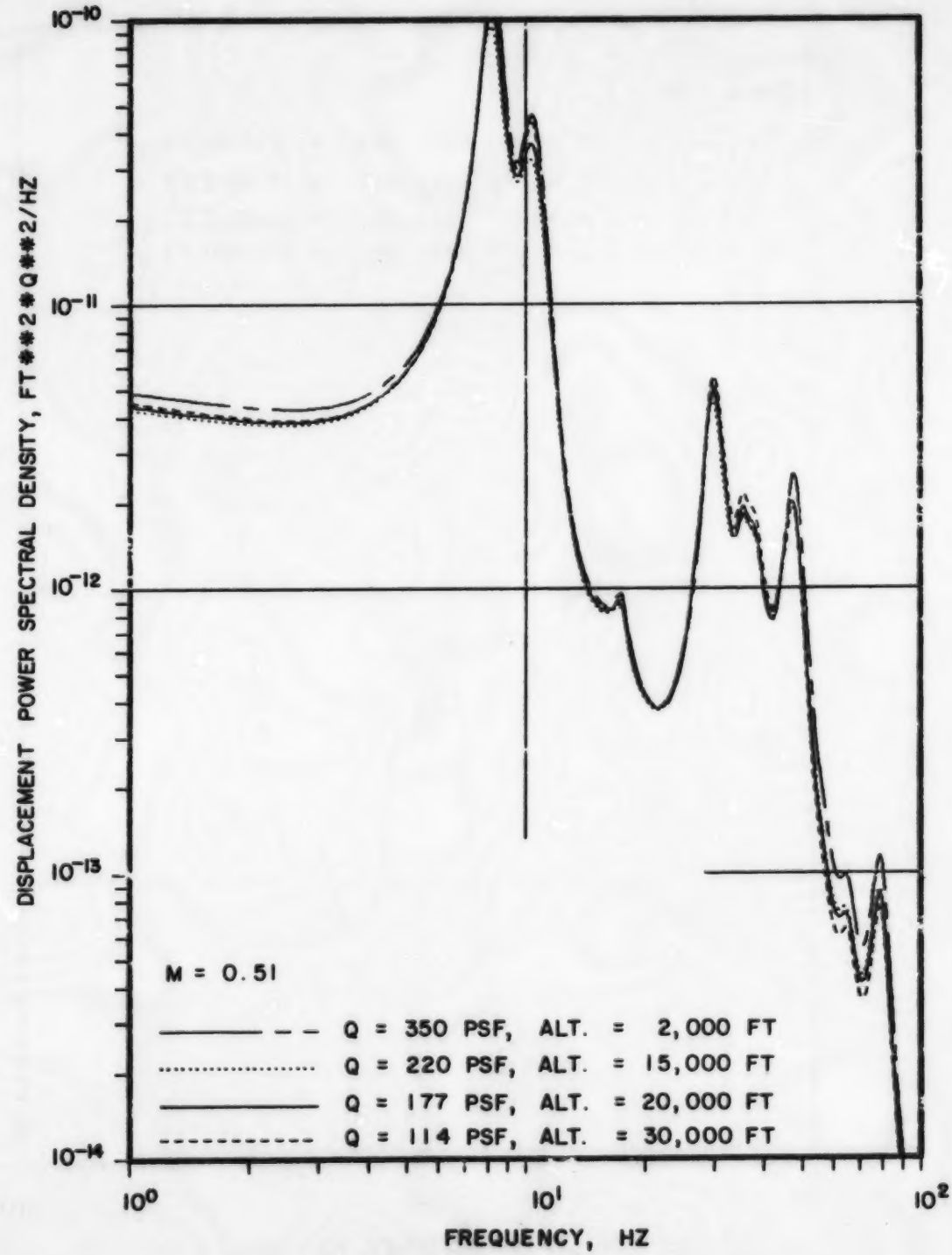

FIG. 20: VARIATION OF DISPLACEMENT POWER SPECTRAL DENSITY NORMALIZED WITH RESPECT TO Q^2 WITH DYNAMIC PRESSURE AND FLIGHT ALTITUDE FOR M = 0.51

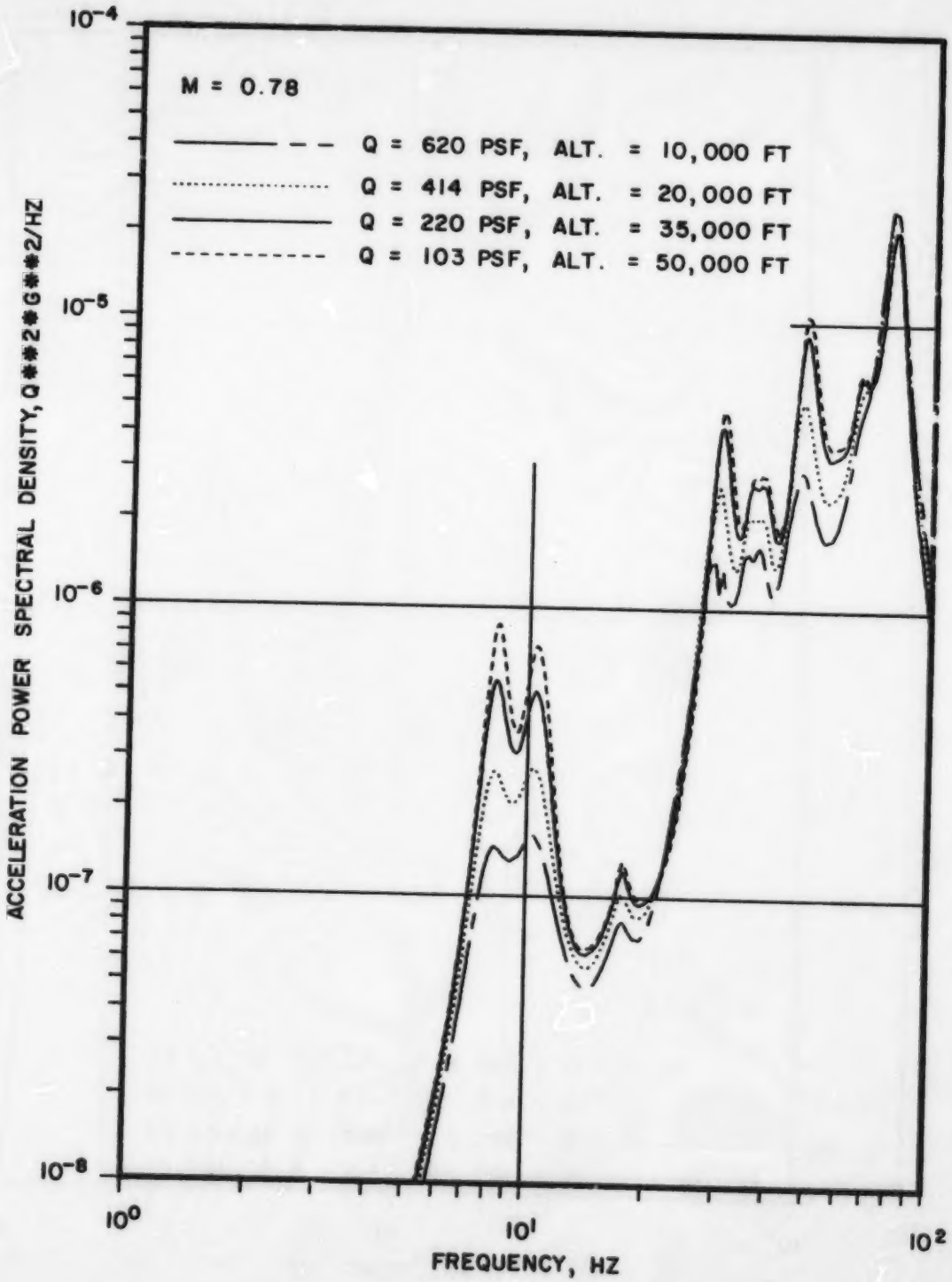

FIG. 21: VARIATION OF ACCELERATION POWER SPECTRAL DENSITY NORMALIZED WITH RESPECT TO Q^2 WITH DYNAMIC PRESSURE AND FLIGHT ALTITUDE FOR M = 0.78

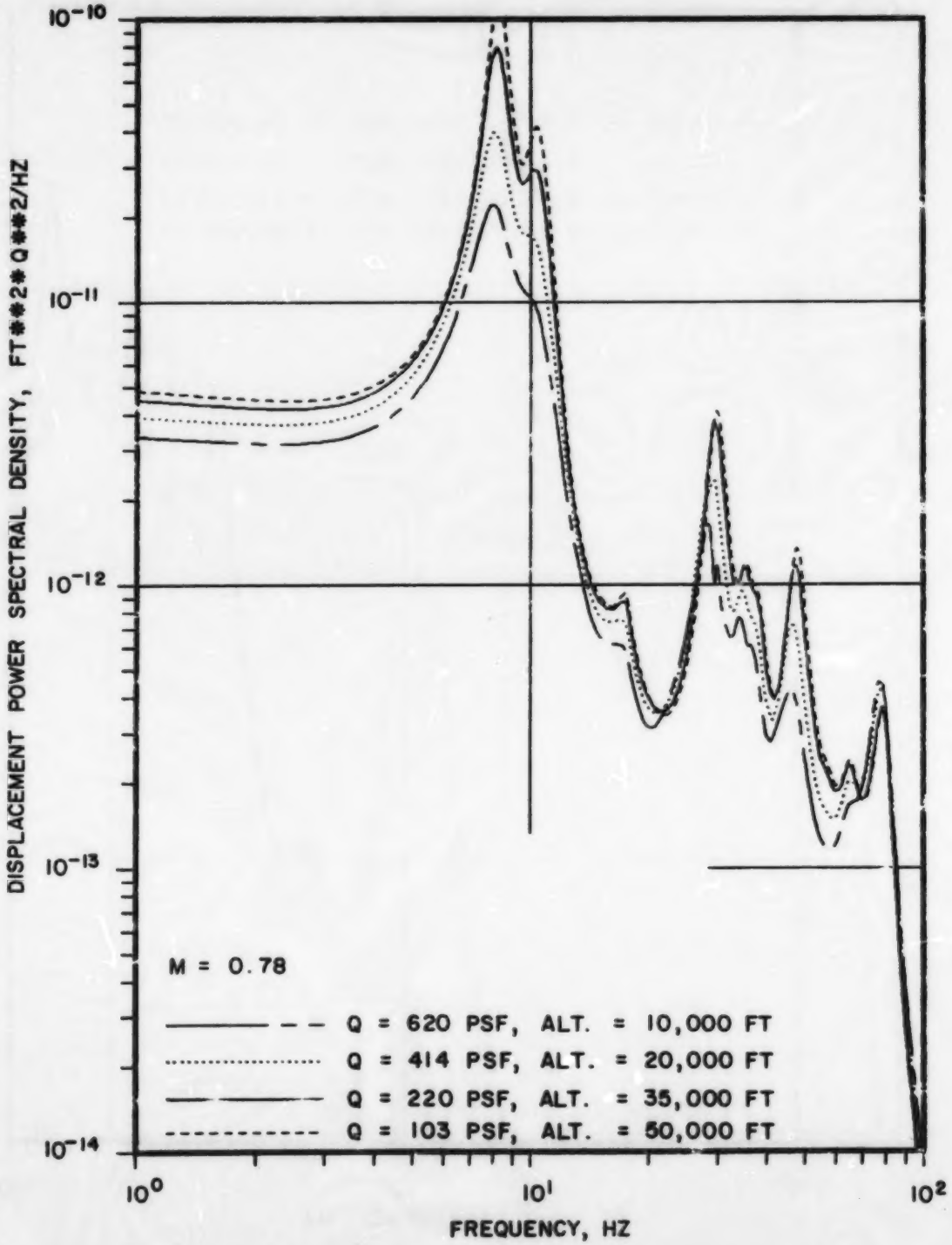

FIG. 22: VARIATION OF DISPLACEMENT POWER SPECTRAL DENSITY NORMALIZED WITH RESPECT TO Q^2 WITH DYNAMIC PRESSURE AND FLIGHT ALTITUDE FOR M = 0.78

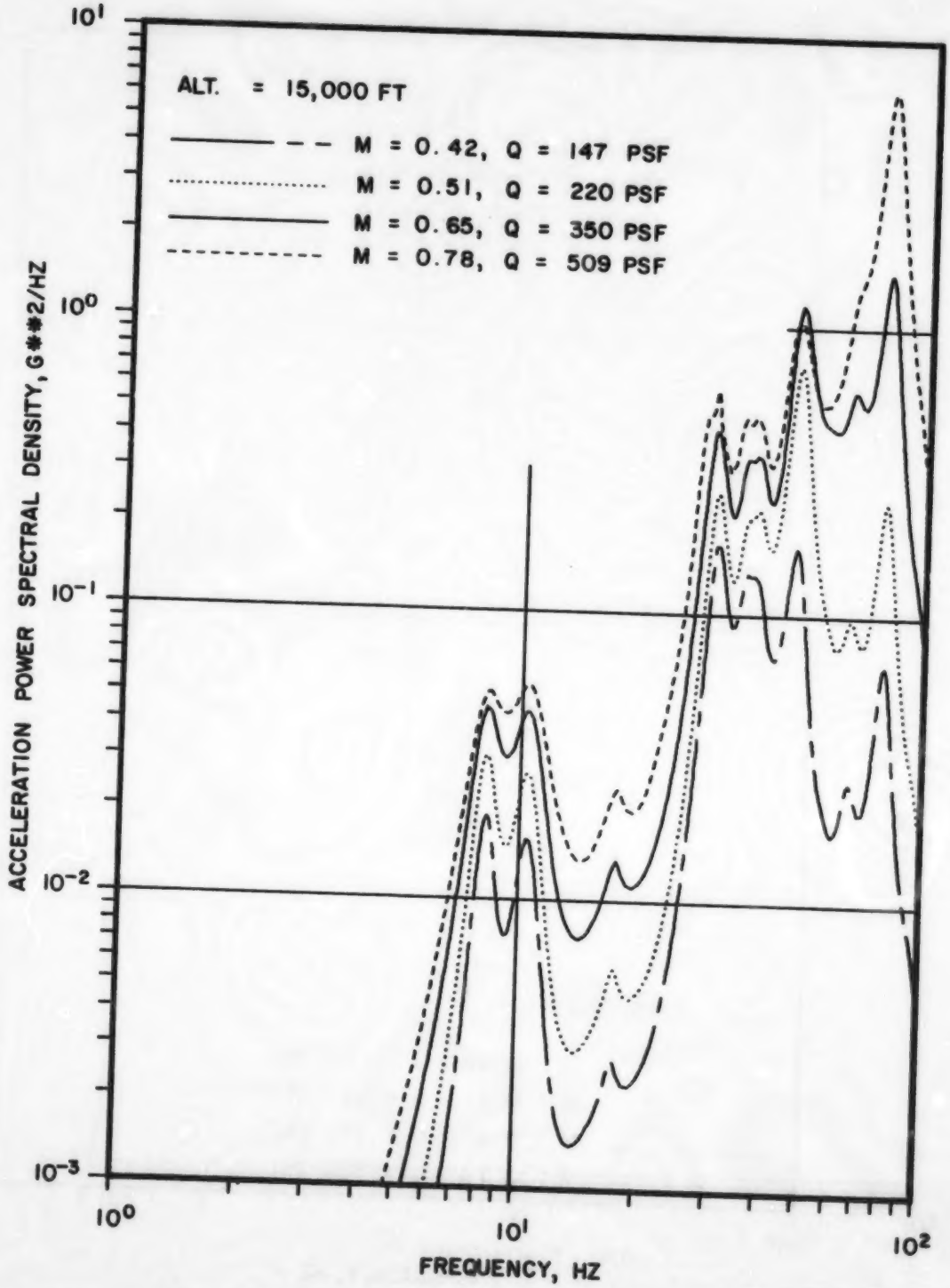

FIG. 23: VARIATION OF ACCELERATION POWER SPECTRAL DENSITY WITH MACH NUMBER AND DYNAMIC PRESSURE AT 15,000 FT. ALTITUDE

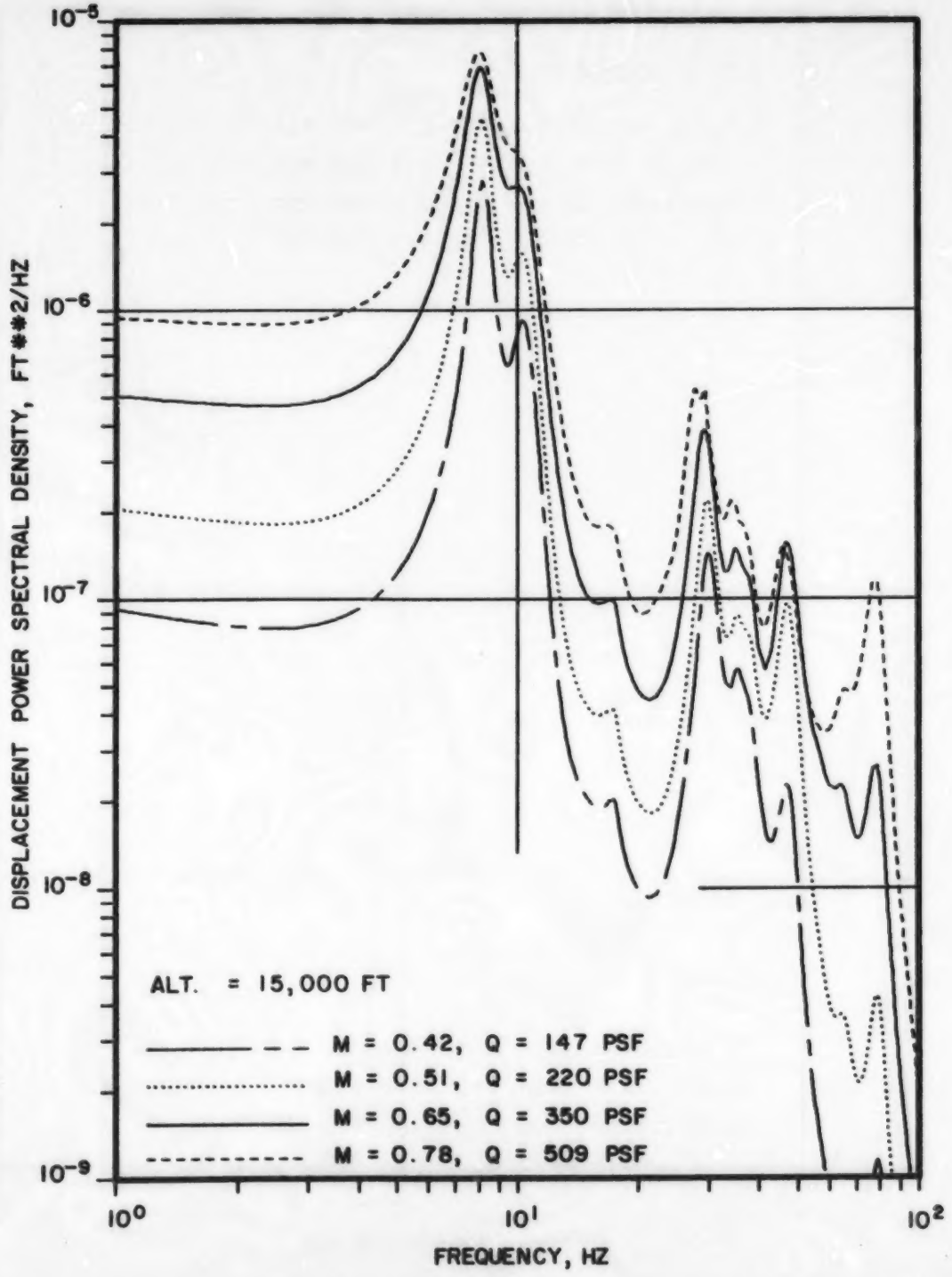

FIG. 24: VARIATION OF DISPLACEMENT POWER SPECTRAL DENSITY WITH MACH NUMBER AND DYNAMIC PRESSURE AT 15,000 FT. ALTITUDE

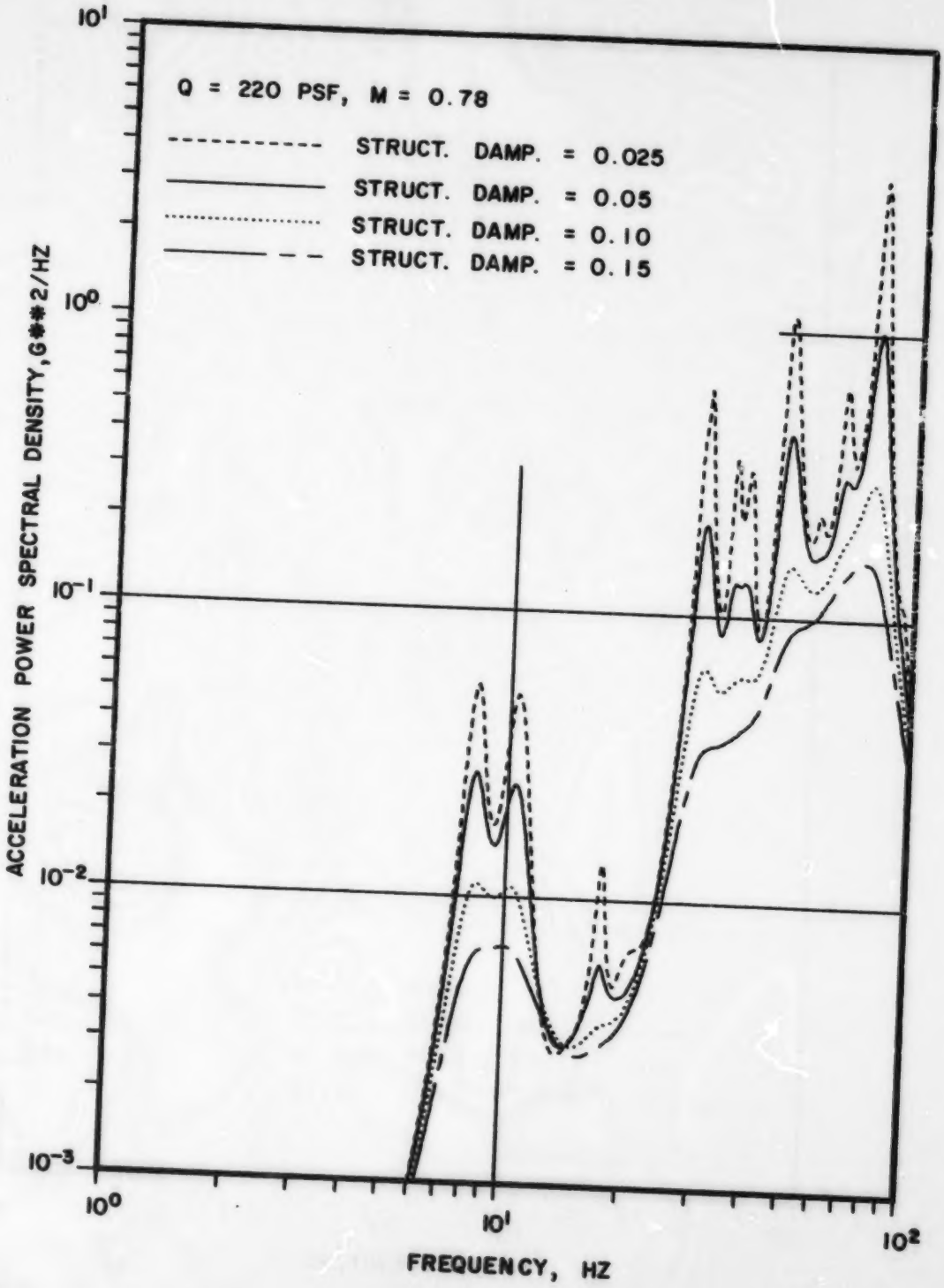

FIG. 25: VARIATION OF ACCELERATION POWER SPECTRAL DENSITY WITH STRUCTURAL DAMPING FOR M = 0.78, Q = 220 PSF

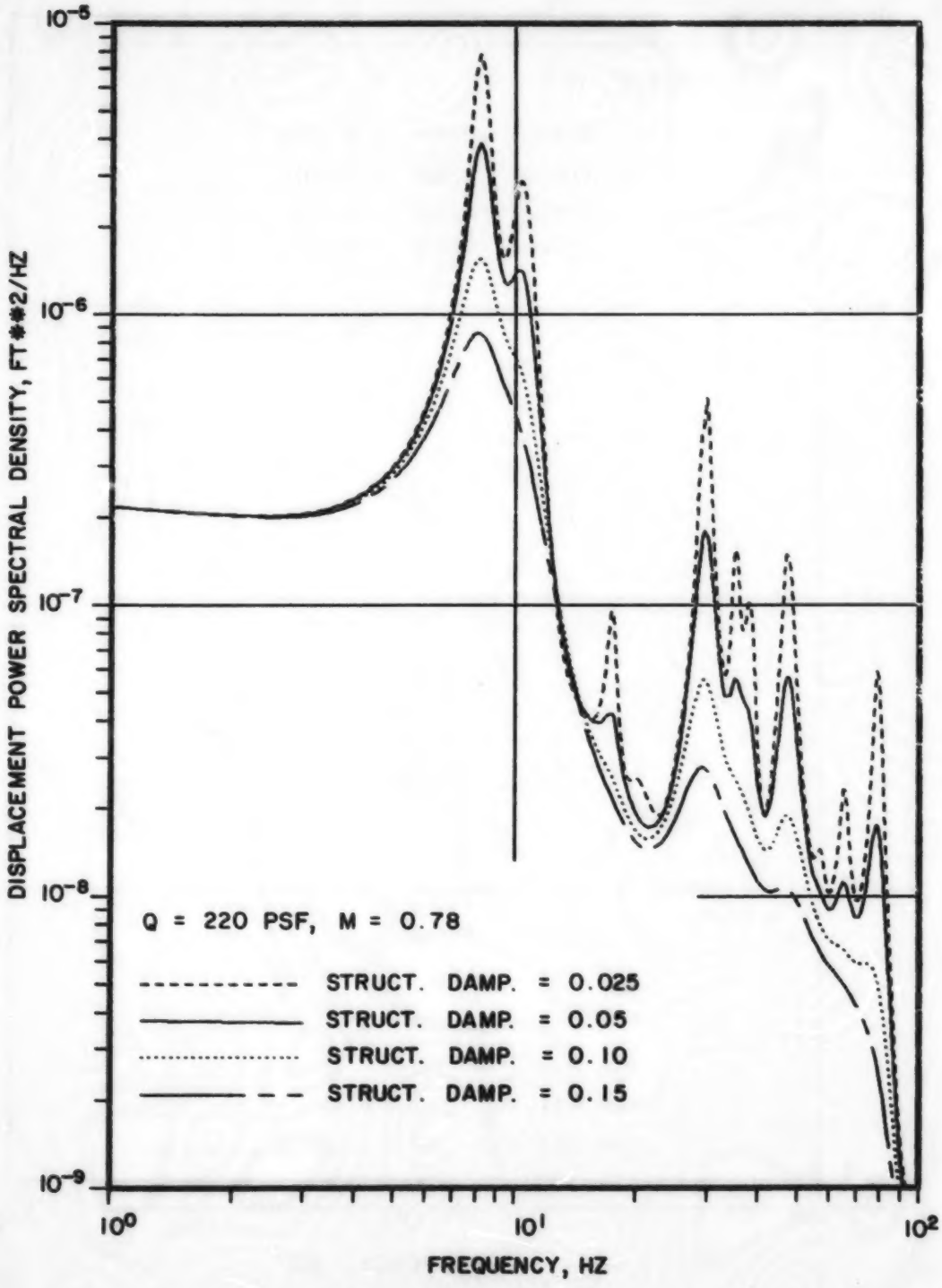

FIG. 26: VARIATION OF DISPLACEMENT POWER SPECTRAL DENSITY WITH STRUCTURAL DAMPING FOR M = 0.78, Q = 220 PSF

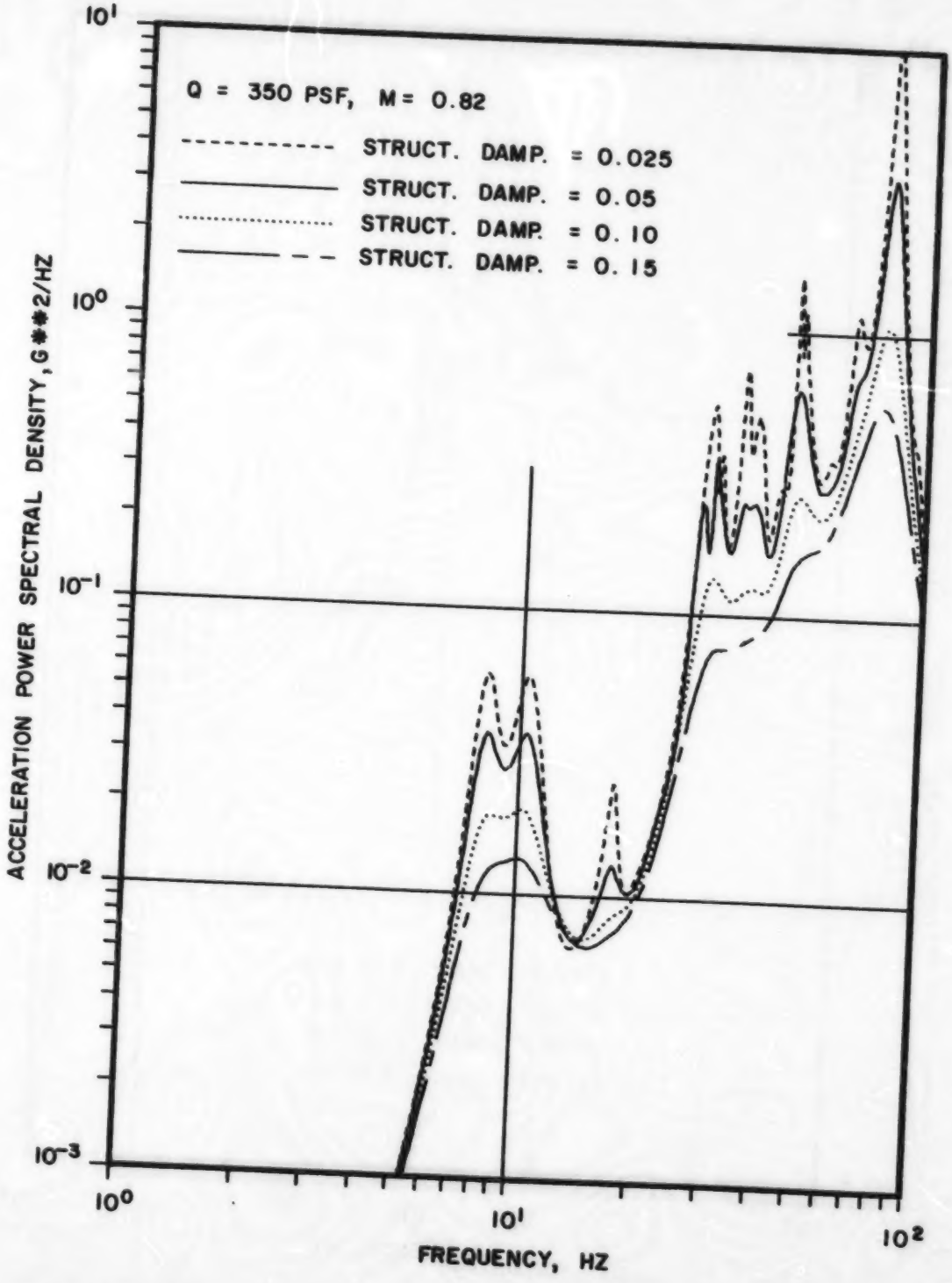

FIG. 27: VARIATION OF ACCELERATION POWER SPECTRAL DENSITY WITH STRUCTURAL DAMPING FOR M = 0.82, Q = 350 PSF

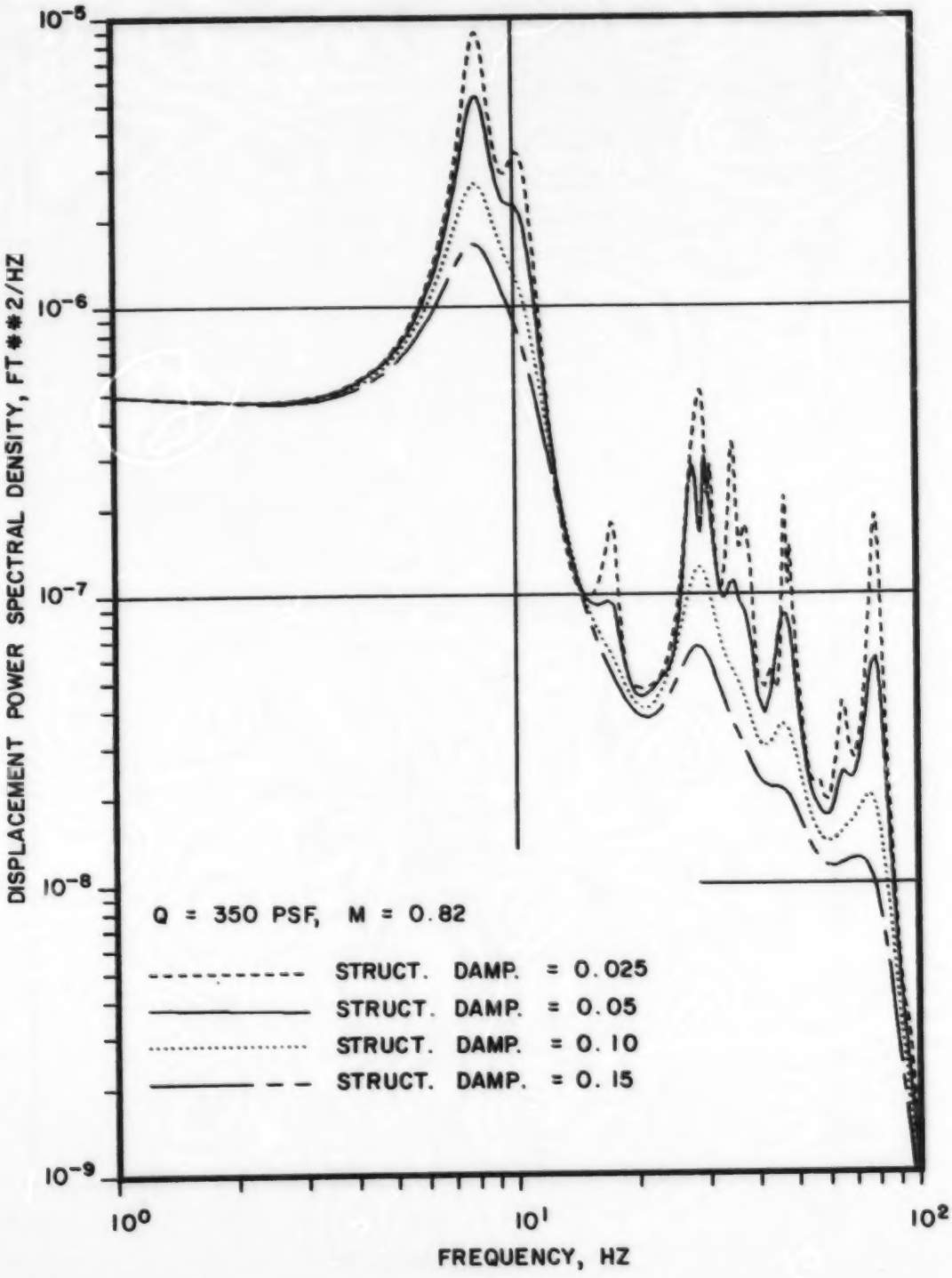

FIG. 28: VARIATION OF DISPLACEMENT POWER SPECTRAL DENSITY WITH STRUCTURAL DAMPING FOR M = 0.82, Q = 350 PSF

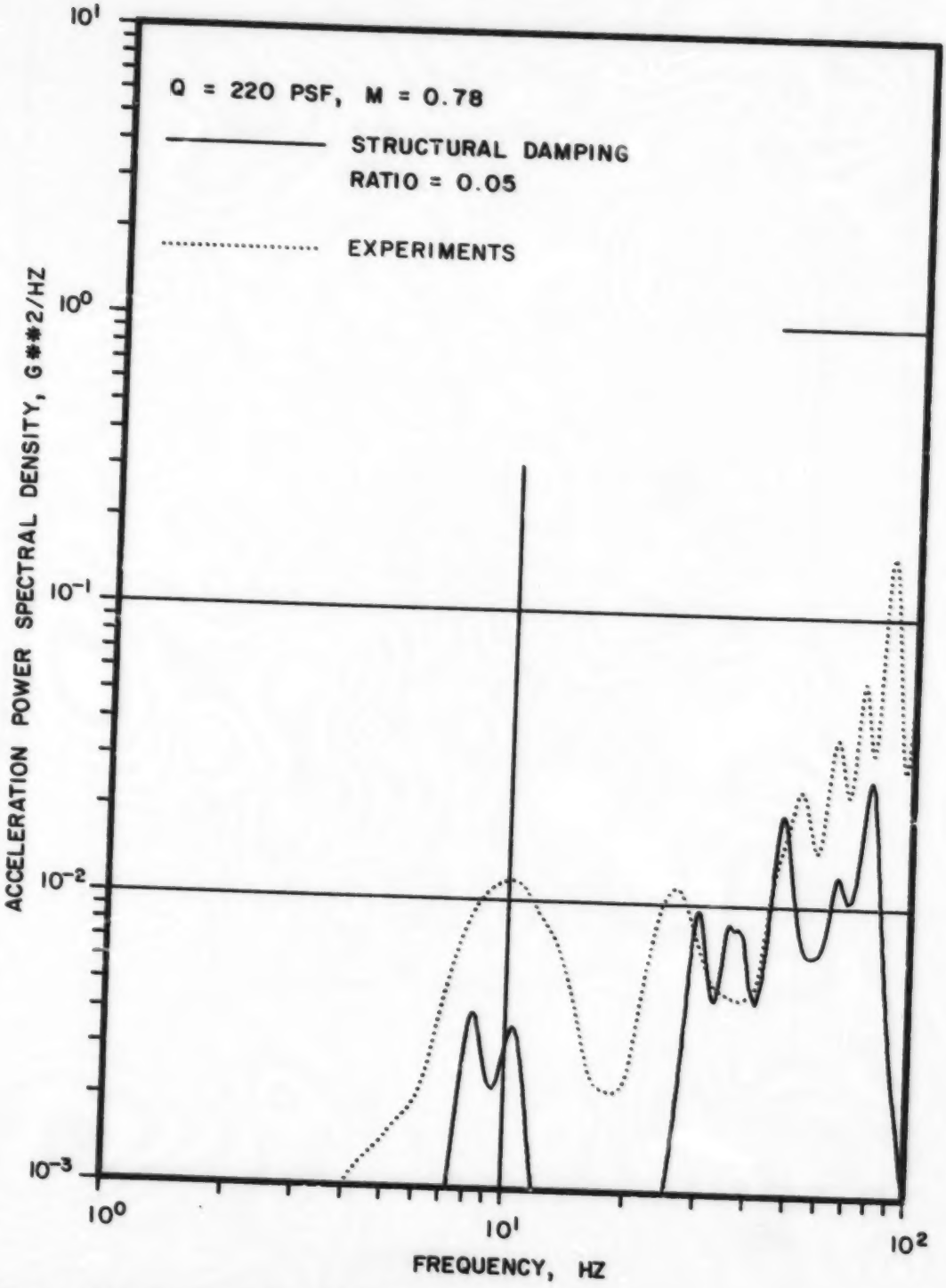

FIG. 29: COMPARISON OF RESPONSE ACCELERATION POWER SPECTRAL DENSITY FROM FLIGHT TESTS WITH THEORETICAL PREDICTIONS USING EXPONENTIAL SPATIALLY DECAYING PRESSURE CROSS-SPECTRUM ASSUMPTION FOR M = 0.78, Q = 220 PF

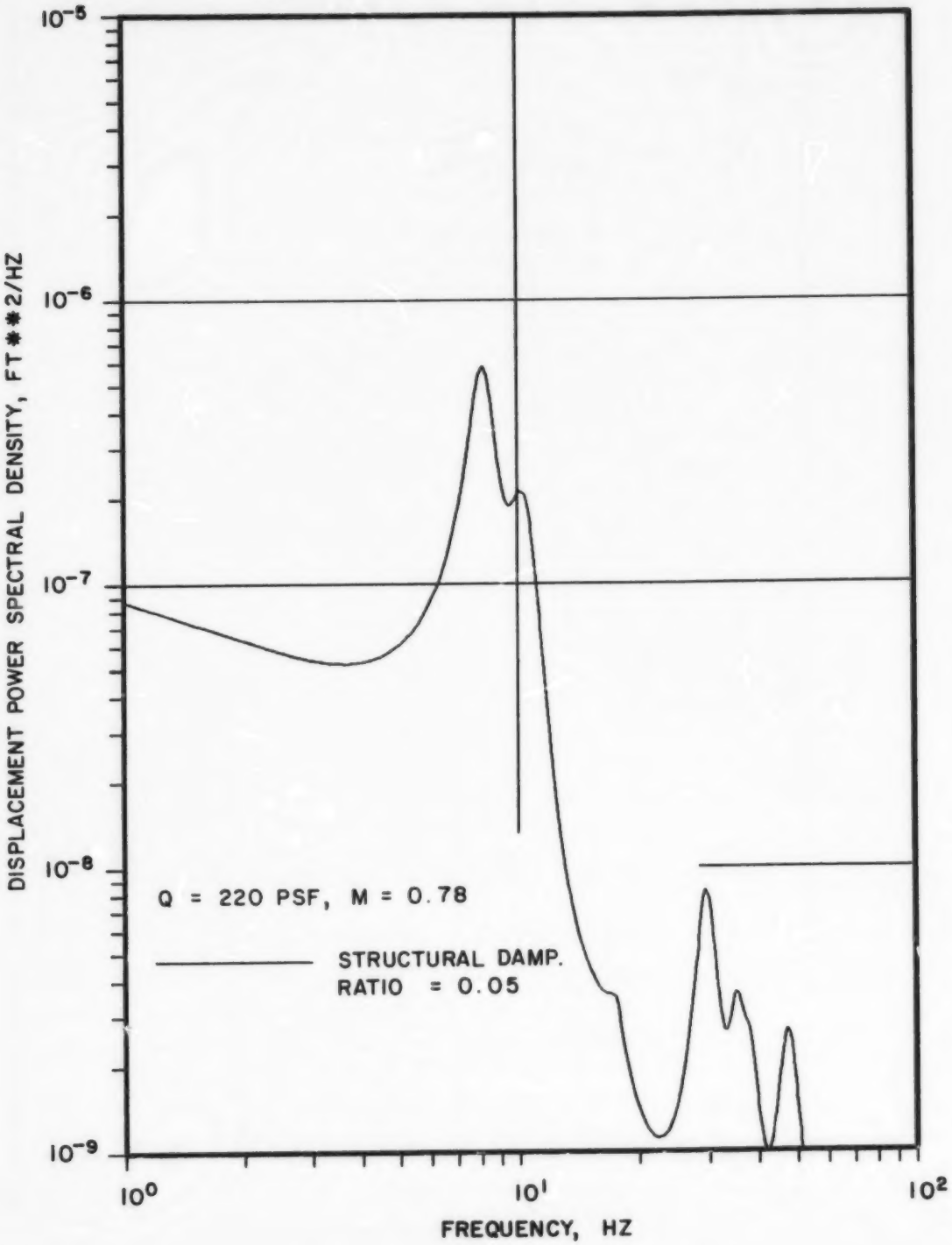

FIG. 30: DISPLACEMENT POWER SPECTRAL DENSITY USING EXPONENTIAL SPATIALLY DECAYING PRESSURE CROSS-SPECTRUM ASSUMPTION FOR M = 0.78, Q = 220 PF

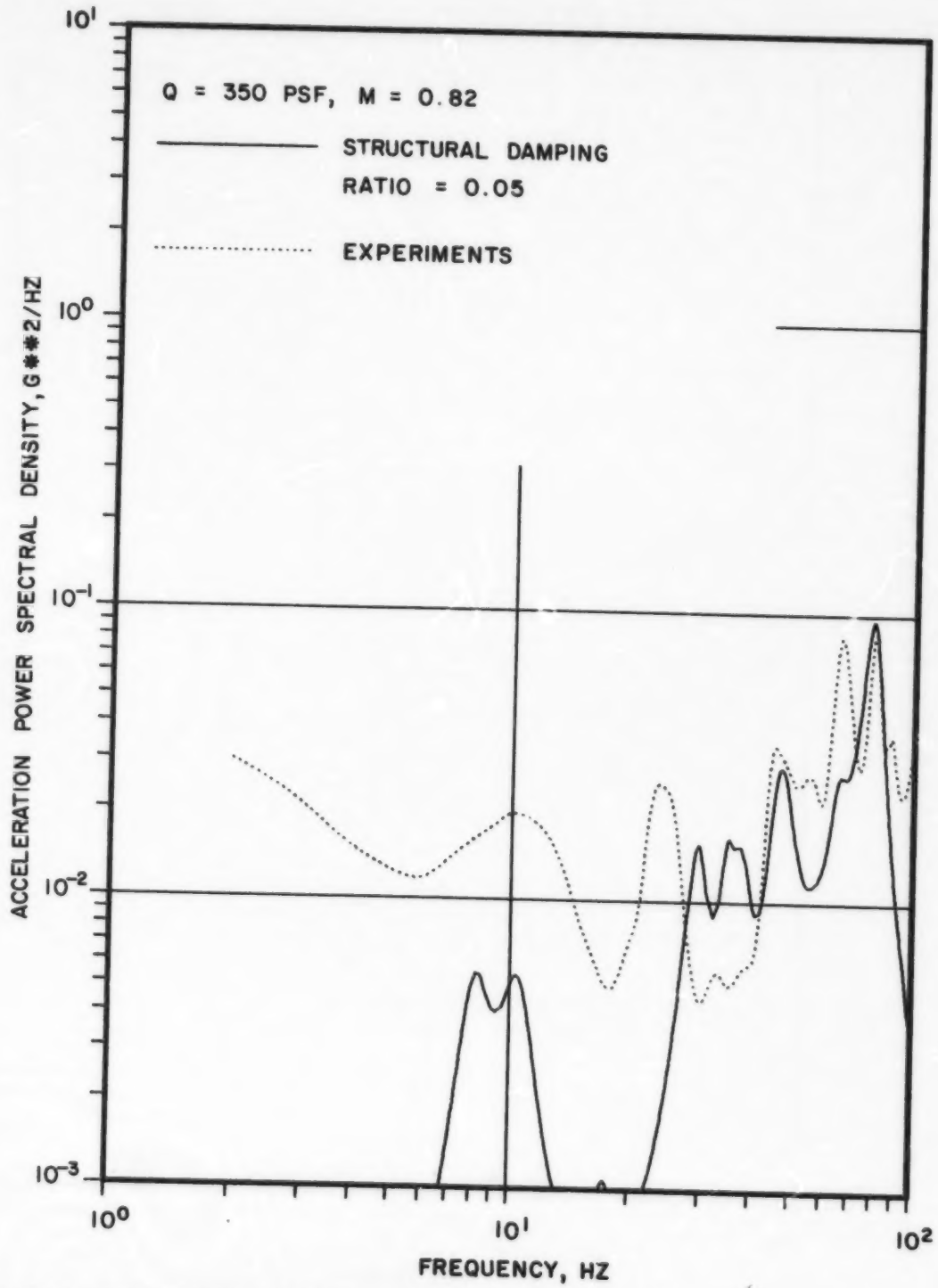

FIG. 31: COMPARISON OF RESPONSE ACCELERATION POWER SPECTRAL DENSITY FROM FLIGHT TESTS WITH THEORETICAL PREDICTIONS USING EXPONENTIAL SPATIALLY DECAYING PRESSURE CROSS-SPECTRUM ASSUMPTION FOR M = 0.82, Q = 350 PSF

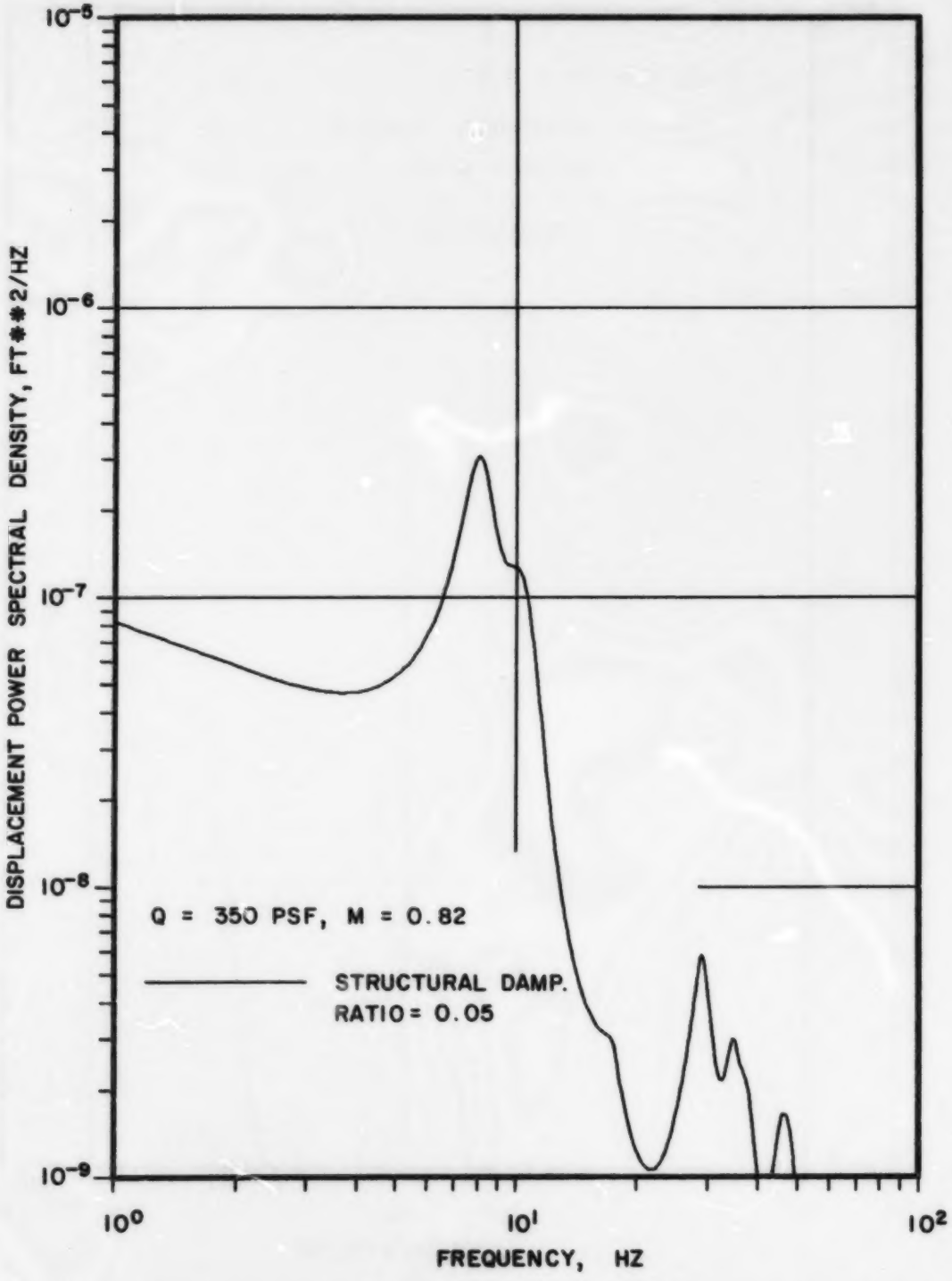

FIG. 32: DISPLACEMENT POWER SPECTRAL DENSITY USING EXPONENTIAL SPATIALLY DECAYING PRESSURE CROSS-SPECTRUM ASSUMPTION FOR M = 0.82, Q = 350 PSF

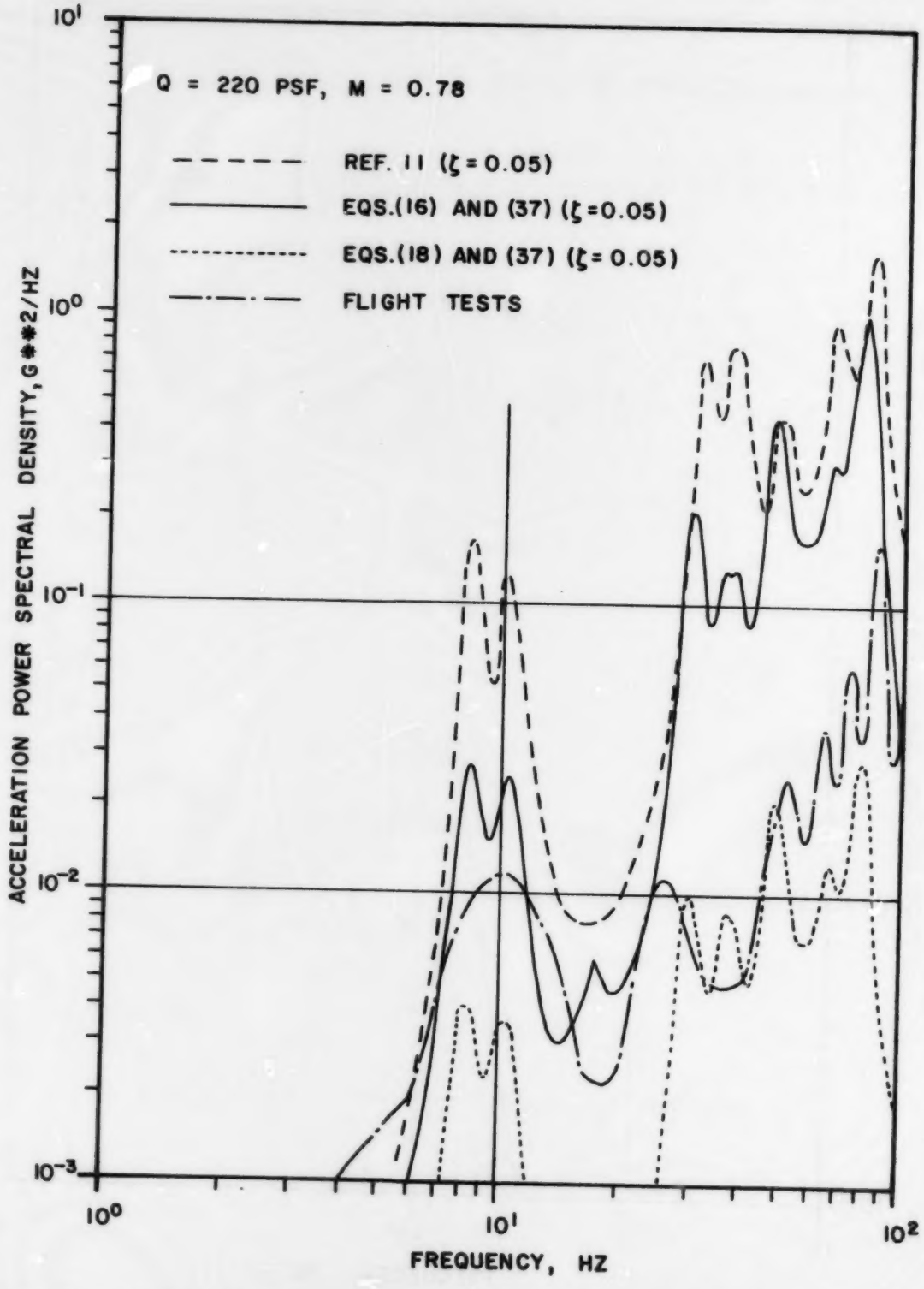

FIG. 33: COMPARISON OF RESPONSE ACCELERATION POWER SPECTRAL DENSITY FROM FLIGHT TESTS WITH THEORETICAL PREDICTIONS FOR M = 0.78, Q = 220 PSF

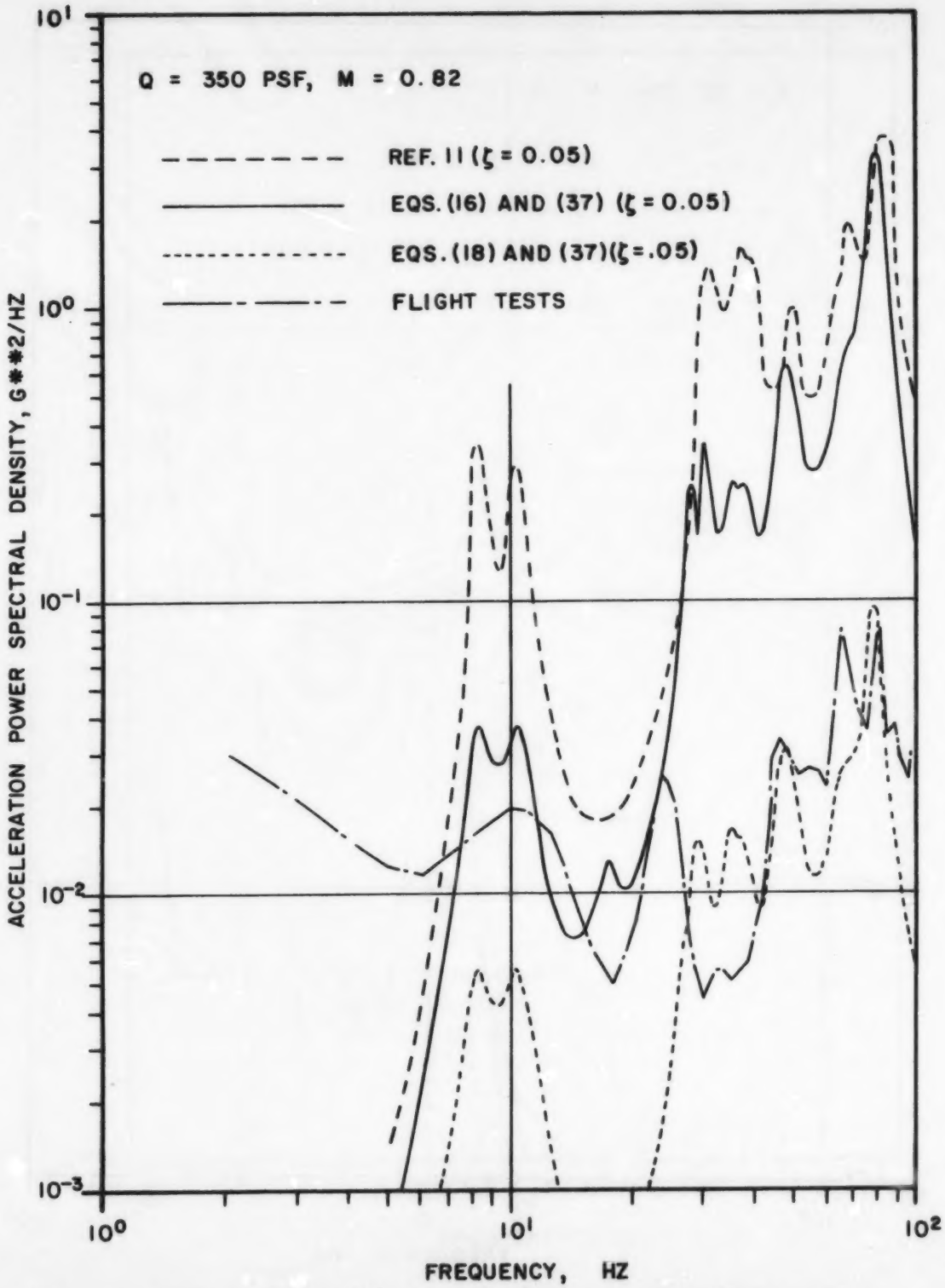

FIG. 34: COMPARISON OF RESPONSE ACCELERATION POWER SPECTRAL DENSITY FROM FLIGHT TESTS WITH THEORETICAL PREDICTIONS FOR M = 0.82, Q = 350 PSF

APPENDIX A

EXPRESSIONS FOR K_1 AND K_2 IN THE EQUATION FOR NORMALWASH

In Equation (21), the terms K_1 and K_2 are given by Landahl (Ref. 20) as follows (with sign reversed):

$$K_1 = -I_1 - \frac{\exp(-ik_1 u_1)Mr_1}{R\left(1+u_1^2\right)^{1/2}} \tag{A1}$$

$$K_2 = 3I_2 + \frac{ik_1 M^2 r_1^2 \exp(-ik_1 u_1)}{R^2\left(1+u_1^2\right)^{1/2}} + \frac{Mr_1}{R}\left[\left(1+u_1^2\right)\frac{\beta^2 r_1^2}{R^2} + 2 + \frac{Mr_1 u_1}{R}\right]\frac{\exp(-ik_1 u_1)}{\left(1+u_1^2\right)^{3/2}} \tag{A2}$$

where

$$\beta = (1-M^2)^{1/2} \tag{A3}$$

$$R = \left[(\bar{x} - \bar{\eta}\tan\lambda_s)^2 + \beta^2 r_1^2\right]^{1/2} \tag{A4}$$

$$U_1 = (MR - \bar{x} + \bar{\eta}\tan\lambda_s)/\beta^2 r_1 \tag{A5}$$

$$k_1 = \frac{\omega r_1}{U} \tag{A6}$$

For $u_1 \geq 0$ (Ref. 19),

$$I_1(u_1,k_1) = \left[1 - \frac{u_1}{\left(1+u_1^2\right)^{3/2}} - ik_1 I_0(u_1,k_1)\right]\exp(-ik_1 u_1) \tag{A7}$$

where

$$I_0(u_1,k_1) \approx \sum_{n=1}^{11} \frac{a_n(nc - ik_1)\exp(-ncu_1)}{n^2c^2 + k_1^2} \tag{A8}$$

$$
\begin{aligned}
a_1 &= 0.2418619 & a_7 &= -41.1863630 \\
a_2 &= -2.7918027 & a_8 &= 545.98537 \\
a_3 &= 24.991079 & a_9 &= -644.78155 \\
a_4 &= -111.59196 & a_{10} &= 328.72755 \\
a_5 &= 271.43549 & a_{11} &= -64.279511 \\
a_6 &= -305.75288 & C &= 0.372
\end{aligned}
\tag{A9}
$$

and
$$
3I_2(u_1,k_1) = \left\{(2 + ik_1u_1)\left(1 - \frac{u_1}{1+u_1^2}\right)^{1/2} - \frac{u_1}{\left(1+u_1^2\right)^{3/2}} - ik_1 I_0(u_1,k_1) + k_1^2 J_0(u_1,k_1)\right\}\exp(-ik_1u_1) \tag{A10}
$$

where

$$
J_0(u_1,k_1) \approx \sum_{n=1}^{11} \frac{a_n \exp(-ncu_1)}{\left(n^2c^2 + k_1^2\right)^2}\left\{n^2c^2 - k_1^2 + ncu_1\left(n^2c^2 + k_1^2\right) - ik_1\left[2nc + u_1\left(n^2c^2 + k_1^2\right)\right]\right\} \tag{A11}
$$

For $u_1 < 0$,

$$
I_1(u_1,k_1) = 2R\ell\, I_1(0,k_1) - R\ell\, I_1(-u_1,k_1) + iI_m I_1(-u_1,k_1) \tag{A12}
$$

and

$$
I_2(u_1,k_1) = 2R\ell\, I_2(0,k_1) - R\ell\, I_2(-u_1,k_1) + iI_m I_1(-u_1,k_1) \tag{A13}
$$

For steady states, K_1 and K_2 are given as:

$$
K_{10} = -1 - (\bar{x} - \bar{\eta}\tan\lambda_s)/R \tag{A14}
$$

$$
K_{20} = 2 + (\bar{x} - \bar{\eta}\tan\lambda_s)\left(2 + \frac{\beta^2 r_1^2}{R^2}\right)/R \tag{A15}
$$

APPENDIX B

EXPRESSIONS FOR NORMALWASH FACTOR

In Equation (25), the normalwash factor is given as:

$$D_{rs} = D_{0_{rs}} + D_{1_{rs}} + D_{2_{rs}} \tag{25}$$

From Reference (21), the steady normalwash factor $D_{0_{rs}}$ can be derived as (Fig. B1):

$$D_{0_{rs}} = \frac{\Delta x_s}{2} (V_y \sin\gamma_r - V_z \cos\gamma_r) \tag{B1}$$

where

$$V_y = (d_{bx}\cos\Lambda\sin\gamma_s - d_{bz}\sin\Lambda) \frac{\cos\theta_b - \cos\varphi_b}{4\pi d_b^2} + \frac{1 - \cos\varphi_i}{4\pi\left(R_{iy}^2 + R_{iz}^2\right)} R_{iz} - \frac{\cos\theta_0 + 1}{4\pi\left(R_{0y}^2 + R_{0z}^2\right)} R_{0z} \tag{B2}$$

and

$$V_z = (d_{by}\sin\Lambda - d_{bx}\cos\Lambda\cos\gamma_s) \frac{\cos\theta_b - \cos\varphi_b}{4\pi d_b^2} - \frac{1 - \cos\varphi_i}{4\pi\left(R_{iy}^2 + R_{iz}^2\right)} R_{iy} + \frac{\cos\theta_0 + 1}{4\pi\left(R_{0y}^2 + R_{0z}^2\right)} R_{0y} \tag{B3}$$

The components of $\vec{d}_b$, $\vec{R}_i$ and $\vec{R}_0$ are:

$$d_{bx} = R_{ix} - R_i\cos\theta_b\sin\Lambda \tag{B4}$$

$$d_{by} = R_{iy} - R_i\cos\theta_b\cos\Lambda\cos\gamma_s \tag{B5}$$

$$d_{bz} = R_{iz} - R_i\cos\theta_b\cos\Lambda\sin\gamma_s \tag{B6}$$

and

$$R_{ix} = X_0 + e\tan\Lambda \tag{B7}$$

$$R_{iy} = y_0 + e\cos\gamma_s \tag{B8}$$

$$R_{iz} = z_0 + e\sin\gamma_s \tag{B9}$$

$$R_{0x} = X_0 - e\tan\Lambda \tag{B10}$$

$$R_{0y} = y_0 - e\cos\gamma_s \tag{B11}$$

$$R_{0z} = z_0 - e\sin\gamma_s \tag{B12}$$

where

$$X_0 = \frac{x_0}{\beta} \tag{B13}$$

$$\tan\Lambda = 1/\beta \tan\lambda_s \tag{B14}$$

$$\beta = \sqrt{1 - M^2} \tag{B15}$$

Finally, the angle relations are given as:

$$\cos\theta_b = \frac{1}{R_i} \left(R_{ix}\sin\Lambda + R_{iy}\cos\Lambda\cos\gamma_s + R_{iz}\cos\Lambda\sin\gamma_s\right) \tag{B16}$$

$$\cos\varphi_b = \frac{1}{R_0} \left(R_{0x}\sin\Lambda + R_{0y}\cos\Lambda\cos\gamma_s + R_{0z}\cos\Lambda\sin\gamma_s\right) \tag{B17}$$

$$\cos\varphi_i = - \frac{R_{ix}}{R_i} \tag{B18}$$

$$\cos\theta_0 = \frac{R_{0x}}{R_0} \tag{B19}$$

From Reference (19), the planar normalwash factor $D_{1_{rs}}$ is given as:

$$D_{1_{rs}} = \frac{\Delta x_s}{8\pi} \left\{ \left[(\bar{y}^2 - \bar{z}^2)A_1 + \bar{y}B_1 + C_1 \right] F + \left(\frac{1}{2} B_1 + \bar{y}A_1 \right) \log \frac{(\bar{y} - e)^2 + \bar{z}^2}{(\bar{y} + e)^2 + \bar{z}^2} + 2eA_1 \right\} \tag{B20}$$

The terms A_1, B_1 and C_1 are determined from the following:

$$A_1 = \frac{1}{2e^2} \left\{ P_1(-e) - 2P_1(0) + P_1(e) \right\} \tag{B21}$$

$$B_1 = \frac{1}{2e} \left\{ P_1(e) - P_1(-e) \right\} \tag{B22}$$

$$C_1 = P_1(0) \tag{B23}$$

where $P_1(e)$, $P_1(-e)$ and $P(0)$ are the outboard, inboard and center values of $P(\bar{\eta})$ defined as:

$$P_1(\bar{\eta}) = T_1 \left\{ K_1 \exp\left[- \frac{i\omega}{U} (\bar{x} - \bar{\eta}\tan\lambda_s) \right] - K_{10} \right\} \tag{B24}$$

which is obtained by subtracting the steady value K_{10} from the numerator of the first term of Equation (21). The term F in Equation (B20) is given by:

$$F = \frac{1}{|\bar{z}|} \tan^{-1} \frac{2e|\bar{z}|}{\bar{y}^2 + \bar{z}^2 - e^2} \tag{B25}$$

where the principal value of the arctangent is taken in the range $(0,\pi)$. When $\bar{z} = 0$,

$$F = \frac{2e}{\bar{y}^2 - e^2} \tag{B26}$$

and for $\bar{z} \ll 1, \bar{y}^2 + z^2 > e^2$,

$$F = \frac{2e}{\bar{y}^2 + \bar{z}^2 - e^2} \left(1 - \alpha \frac{\bar{z}^2}{e^2}\right) \tag{B27}$$

and

$$\alpha \approx \frac{4e^4}{(\bar{y}^2 + \bar{z}^2 - e^2)^2} \sum_{n=2}^{7} \frac{(-1)^n}{2n-1} \left(\frac{2e\bar{z}}{\bar{y}^2 + \bar{z}^2 - e^2}\right)^{2n-4} \tag{B28}$$

The non-planar normalwash factor $D_{2_{rs}}$ is:

$$\begin{aligned} D_{2_{rs}} = \frac{\Delta x_s}{16\pi\bar{z}^2} \Bigg\{ & \left[(\bar{y}^2 + \bar{z}^2)A_2 + \bar{y}B_2 + C_2\right]F \\ & + \frac{1}{(\bar{y}+e)^2 + \bar{z}^2} \Big(\left[(\bar{y}^2 + \bar{z}^2)\bar{y} + (\bar{y}^2 - \bar{z}^2)e\right]A_2 + (\bar{y}^2 + \bar{z}^2 + \bar{y}e)B_2 \\ & + (\bar{y}+e)C_2 \Big) - \frac{1}{(\bar{y}-e)^2 + \bar{z}^2} \Big(\left[(\bar{y}^2 + \bar{z}^2)\bar{y} - (\bar{y}^2 - \bar{z}^2)e\right]A_2 \\ & + (\bar{y}^2 + \bar{z}^2 - \bar{y}e)B_2 + (\bar{y} - e)C_2 \Big) \Bigg\} \end{aligned} \tag{B29}$$

A_2, B_2 and C_2 are determined from Equations (B21) to (B24) with the subscripts in those equations changed to '2'. For small values of $\bar{z}$, the following equation for $D_{2_{rs}}$ is used:

$$D_{2_{rs}} = \frac{\Delta x_s e}{8\pi(\bar{y}^2 + \bar{z}^2 - e^2)} \left\{ \frac{2(\bar{y}^2 + \bar{z}^2 + e^2)(e^2 A_2 + C_2) + 4\bar{y}e^2 B_2}{\left[(\bar{y}+e)^2 + \bar{z}^2\right]\left[(\bar{y}-e)^2 + \bar{z}^2\right]} - \frac{\alpha}{e^2}\left[(\bar{y}^2 + \bar{z}^2)A_2 + \bar{y}B_2 + C_2\right] \right\} \tag{B30}$$

where α is given by Equation (B28). This equation is generally used except when $(\bar{y}^2 + \bar{z}^2 - e^2)/2e\bar{z} < 0.1$ in which case Equation (B29) is used instead.

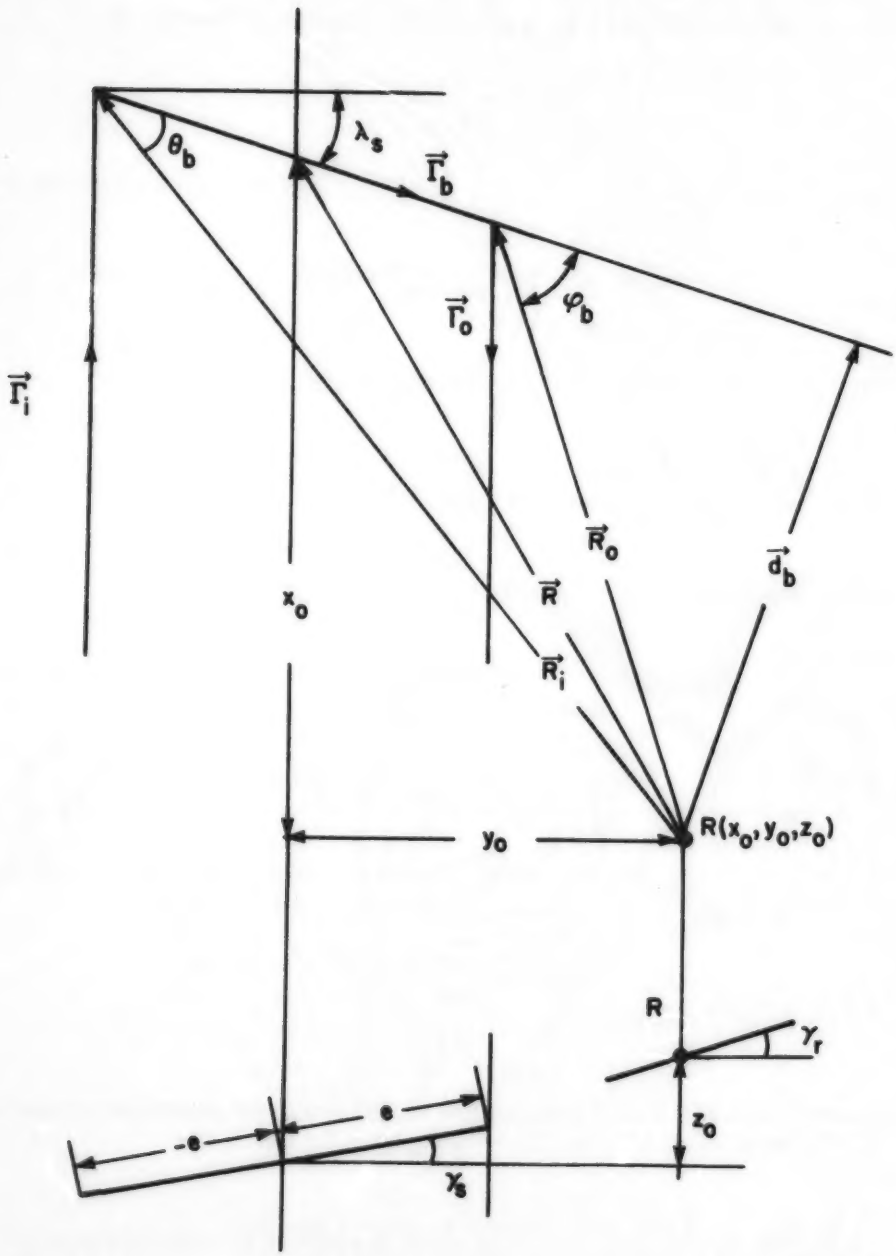

FIG. B1: HORSESHOE VORTEX SYSTEM

REPORT DOCUMENTATION PAGE / PAGE DE DOCUMENTATION DE RAPPORT

REPORT/RAPPORT 1a	REPORT/RAPPORT 1b
LR-613	NRC No. 21230
REPORT SECURITY CLASSIFICATION / CLASSIFICATION DE SÉCURITÉ DE RAPPORT 2	**DISTRIBUTION (LIMITATIONS)** 3
Unclassified	Unlimited

TITLE/SUBTITLE/TITRE/SOUS-TITRE 4

Aeroelastic Response of an Aircraft Wing to Random Loads

AUTHOR(S)/AUTEUR(S) 5

B.H.K. Lee

SERIES/SÉRIE 6

Aeronautical Report

CORPORATE AUTHOR/PERFORMING AGENCY/AUTEUR D'ENTREPRISE/AGENCE D'EXÉCUTION 7

National Research Council Canada
National Aeronautical Establishment — High Speed Aerodynamics Laboratory

SPONSORING AGENCY/AGENCE DE SUBVENTION 8

DATE 9	FILE/DOSSIER 10	LAB. ORDER / COMMANDE DU LAB. 11	PAGES 12a	FIGS/DIAGRAMMES 12b
83-04			60	34

NOTES 13

DESCRIPTORS (KEY WORDS)/MOTS-CLÉS 14

1. Wings — load distribution
2. Wings — test results

SUMMARY/SOMMAIRE 15

A method for the prediction of the response of an elastic wing to random loads at flight conditions using rigid model wind tunnel pressure fluctuation measurements is presented. The wing is divided into panels or elements, and the load is computed from measured pressure fluctuations at the centre of each panel. A series representation with terms of the correlated noise type is used to curve fit the experimentally determined pressure power spectra. Two methods are used to calculate the random load spectrum: a constant correlation approximation, and an exponential spatially decaying cross-power spectrum model for the pressure. The coupling between the structural dynamics and aerodynamics of a vibrating wing is taken into consideration using the doublet-lattice method for computing the unsteady aerodynamic forces. The acceleration and displacement response spectra have been computed for the F-4E aircraft for various Mach numbers, dynamic pressures and flight altitudes. The importance of the unsteady aerodynamic loads induced by the vibration of the wing and input load representation is illustrated by comparing the theoretical predictions with results from flight tests.